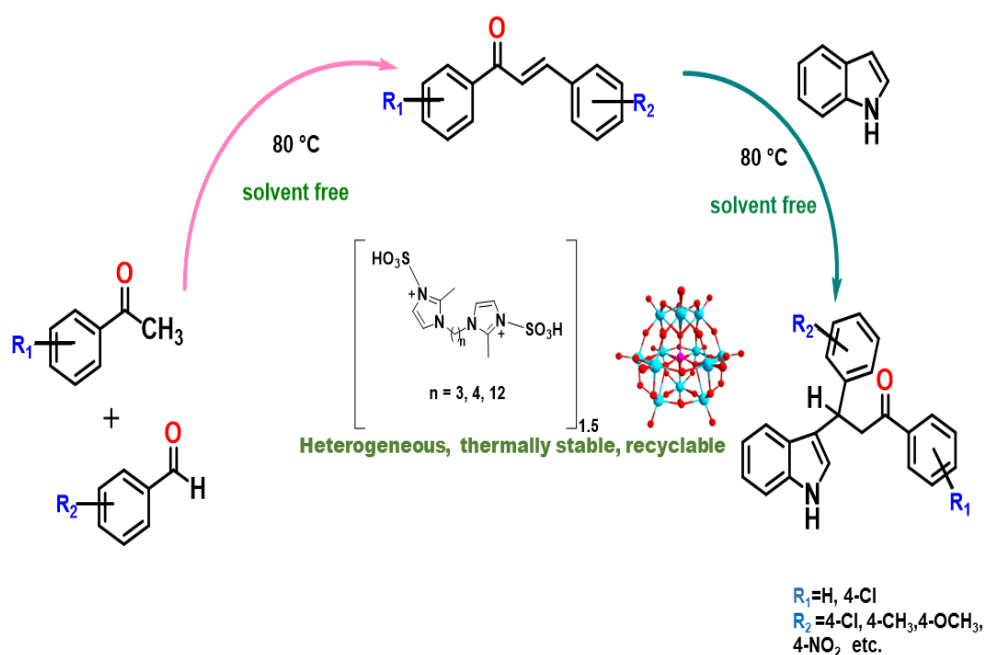


Chapter-4

Study of catalytic activity of methylene bridged dicationic -SO₃H functionalized imidazolium phosphomolybdate hybrids for one pot sequential synthesis of 3-substituted indoles



Synopsis: Assembly of $\text{-SO}_3\text{H}$ functionalized dicationic imidazolium ionic-liquids having variable lengths of methylene connecting spacers with inorganic Keggin phosphomolybdic acid provide heterogeneous nature to the synthesized hybrids making them easily recyclable and thermally stable acidic catalyst. The one with the longest methylene connecting spacer was found to be more efficient as an acid catalyst towards solvent-free one-pot Michael-like addition of indole with chalcones obtained via Claisen-Schmidt condensation.

4.1 Introduction

One of the noteworthy reactions in organic chemistry involving the formation of C-C, C-N and C-S bonds is Michael addition which occurs *via* conjugate addition of nucleophiles to unsaturated carbonyl compounds in the presence of acidic or basic catalysts [1]. The importance of heterocyclic scaffolds and their association with drug-discovery studies has brought remarkable attention to their clean and effective synthesis procedure [2, 3]. Studies on indole nuclei are increasing as it possesses numerous pharmacological qualities including antibiotic [4], anticancer [5], anti-bacterial [6], central nervous system modulating [7] etc. For example, yohimbin (17 α -hydroxy-yohimban-16 α -carboxylic acid methyl ester), an indole alkaloid is used as a drug molecule for the treatment of sexual dysfunction [8] and also explored as a remedy for type 2 diabetes in animal [9]. Oxypertine and arbidol are another two indole derivatives used in the treatment of schizophrenia [10] and used as antiviral [11] respectively. Likewise, chalcones are also one of the crucial biologically active compounds. They are seen to have properties like cytotoxic [12], antimalarial [13] antileishmanial [14], anti-inflammatory [15], anti-HIV [16] antifungal [17] etc. Similarly, chalcones with naphthalene moiety have also been reported as potent anticancer agents [18]. Structures of a few pharmacologically important 3-substituted indole derivatives are provided in **Fig. 1A.9, Chapter 1A, section 1A.8**.

Keeping in view the capable prospects of these molecules, many attempts have been made by researchers to synthesize molecules containing both moieties in a single framework [19]. Likewise, the synthesis of 3-substituted indole derivatives *via* Michael like addition of indoles to chalcones has also been attracting interest of chemists for many decades. Conventionally, α , β -unsaturated ketones as one of the substrates are utilized by many researchers for conjugate addition with the indoles using various catalysts like SbCl_3 , GaI_3 , polyvinyl sulfonic acid, ceric ammonium nitrate, p-toluene sulfonic acid,

InCl_3 , $\text{CeCl}_3 \cdot 7\text{H}_2\text{O}$ - NaI supported on silica gel [19–25]. However, many of these above-given procedures bear shortcomings such as long reaction time, use of toxic reagents, formation of side products and use of hazardous solvents. Few reports are also present using ionic liquids as catalysts for such reactions and one such work was done by our group in which $-\text{SO}_3\text{H}$ functionalized ionic liquid catalyst was used as liquid catalyst for the synthesis of 3-substituted indoles [26,27].

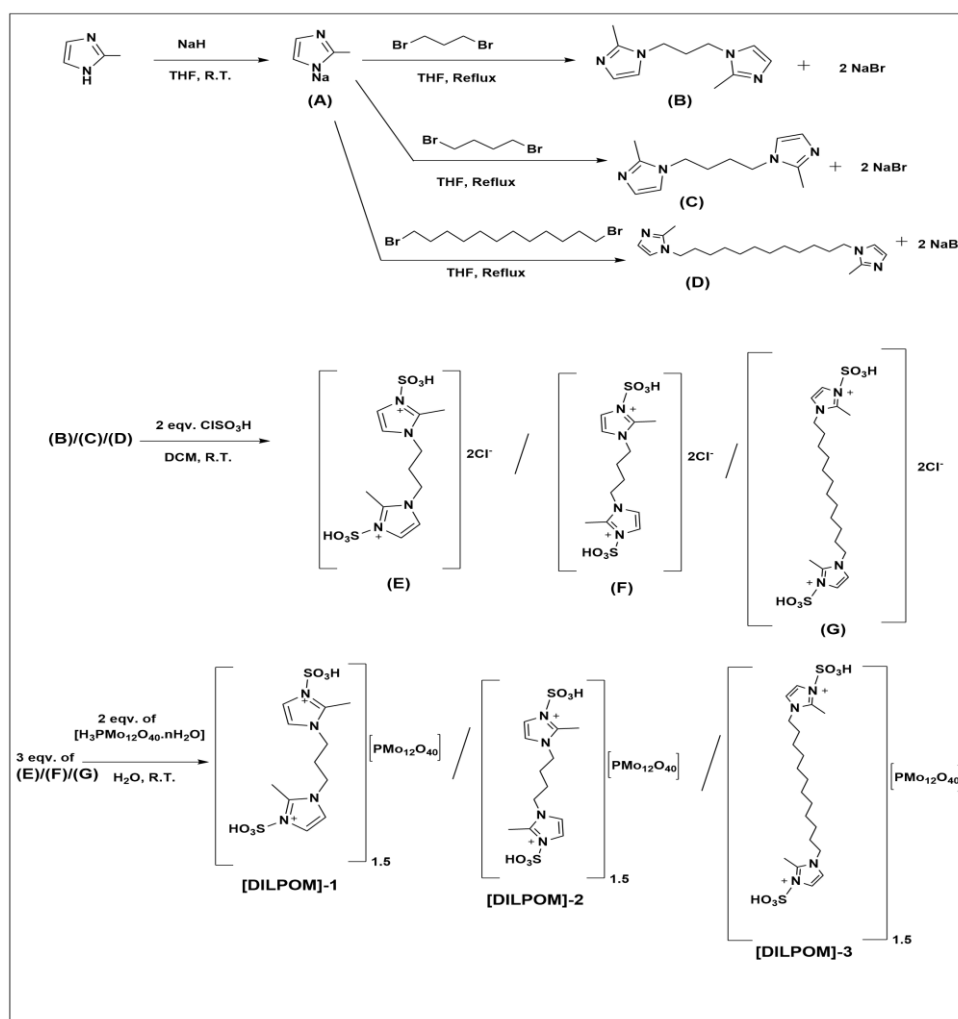
Polyoxometalates (POMs) represent anionic species of metal and oxygen with large molecular weights, range of sizes, nuclearities etc. These are a large family of metal-oxygen cluster compounds with very high thermal stability and the inorganic-cage type anions having Keggin structure are of the form $[\text{XM}_{12}\text{O}_{40}]^{n-}$, where X is the heteroatom (e.g., P^{5+} or Si^{4+}) and M is the addendum atom (W^{6+} or Mo^{6+}) and these have been used extensively for acid catalysed reactions [28, 29]. Extensive advancement in POM chemistry based on their unique properties has been achieved in many fields like photochromism, separation chemistry, electrochemistry, magnetism and especially catalysis [30-35]. Keggin type of POMs has been employed in various applications [36-39] and their performance as good catalysts is a consequence of their high thermal stability, presence of different active sites like protic acid, oxygen, and metals [40]. POMs and their high activity in acid-catalysed reactions are mainly because of the presence of protons and unoccupied metal orbitals [35]. 12-Tungstoboric acid ($\text{H}_5\text{BW}_{12}\text{O}_{40}$) is used as an efficient homogeneous Lewis acid catalytic system for synthesis of pharmacologically active compounds, chromenopyrimidine-2,5-diones and thioxochromenopyrimidin-5-ones [41]. However, the high solubility of POMs and thus their use as homogeneous catalysts with limitations like separation of products and catalysts, poor recyclability in many cases, has restricted their use in industries [42]. Accordingly, different approaches to generation of heterogeneous catalysts out of POMs have attracted much interest. One way is the immobilization of POMs on solid surfaces [43-45] and the other one is generation of POM-based hybrids by ion exchange with specific cations [46]. Immobilization of POMs on various supports like zeolite is effective with large surface area but due to hydrophilicity in the framework, it restricts the interaction of hydrophobic substrates to the active sites [47,48]. And there are a lot of incidences of heavy leaching due to weak interaction between POMs and support which acts as demerit to such systems [42]. While designing POM-based heterogeneous catalysts, properties like water tolerance, adjustable polarity should be considered [42]. Heterogeneous Lacunary POM derived hybrids based catalytic

systems were synthesized by groups of researchers like $(\text{TBA})_7[\text{PW}_{11}\text{O}_{39}]$, $(\text{TBA})_8[\text{SiW}_{11}\text{O}_{39}] \cdot 4\text{H}_2\text{O}$, $(\text{TBA})_9[\text{BW}_{11}\text{O}_{39}] \cdot 11\text{H}_2\text{O}$ and $(\text{TBA})_6[\text{Zr}(\text{OH})\text{BW}_{11}\text{O}_{39}] \cdot 8\text{H}_2\text{O}$, where (TBA^+) : tetrabutylammonium) and were used for organic synthesis reactions [49,50]. Inorganic–organic hybrids like $[\text{Dy}_4(\text{PDA})_4(\text{H}_2\text{O})_{11}(\text{SiMo}_{12}\text{O}_{40})] \cdot 7\text{H}_2\text{O}$, $\text{Na}[\text{Nd}(\text{pydc-OH})(\text{H}_2\text{O})_4]_3[\text{SiW}_{12}\text{O}_{40}]$, $[\text{Co}_2(\text{C}_4\text{H}_6\text{NO}_4)_2(\text{Mo}_8\text{O}_{26})(\text{H}_2\text{O})_{10}] \cdot 4\text{H}_2\text{O}$ are another three catalysts derived from polyoxometalates used for synthesis of 2-amino-4H-chromene derivatives, [pyrazolo]pyrido[2,3-d]pyrimidine- diones, functionalized spirochromenes respectively through multicomponent reaction [35, 51, 52]. The combination of d and f metal ions into the lacunary site of POMs is another strategy for preparing POM-based heterogeneous catalysts with improvement in the catalytic activity of POMs. $[\text{Nd}(\text{H}_2\text{O})_8][\text{Ag}\{\text{Nd}(\text{H}_2\text{O})_6\}_2\{\text{SiW}_{11}\text{Nd}(\text{H}_2\text{O})_4\text{O}_{39}\}_2] \cdot 6\text{H}_2\text{O}$ is such a pure inorganic heterogeneous catalyst which was used to check its catalytic activity for synthesis of different polyhydroquinolines and pyrimidines via Hantzsch and Bignelli reactions [53]. Series of Ln-POMs $\text{K}_{15}[\text{Ln}(\text{BW}_{11}\text{O}_{39})_2]$ (Ln=B₂W₂₂, Ln=La, Ce, Nd, Sm, Gd, and Er) was developed and used for synthesis of bioactive isatin derivatives and another series of $[\text{Ln}(\text{W}_5\text{O}_{18})_2]^{9-}$ (Ln = La, Ce, Nd, Gd, Tb) was developed and used for synthesis of pyrazolopyranopyrimidines by the same group, Mirzaei and Heravi et al. [54, 55].

Generally, liquid acid catalysts like mineral acids and $-\text{SO}_3\text{H}$ functionalized ionic liquids show good activity, but the hazardous acidic fumes of acid catalysts cause environmental problems apart from their strong corrosive nature. And the product isolation also becomes tedious [56]. Therefore, POM anions combined with task-specific ionic liquids, provide a strong option for resolving the solubility issue of POMs in polar solvents and generation of efficient and cleaner technology compared to polluting and corrosive liquid acid catalysts. The role of counter-cations of the precursor ionic liquid is immense in deciding the resultant nature of the hybrid. Hybrids based on polyoxometalate with large cationic counter ion result in insoluble catalysts and this type of catalysts thus falls under heterogeneous catalysts.

From this perspective, synthesizing organic-inorganic hybrid materials from specially designed organic dications with the $\text{PMo}_{12}\text{O}_{40}^{3-}$ anion can address the need for catalysts being heterogeneous with better properties. Dicationic ionic liquids were chosen as precursors for synthesis of the hybrids used in this work as they show several advantages like better thermal stability, lower volatility etc. over monocationic ionic

liquids [57]. Therefore, it was aimed to design the organic cations varying the methylene chain length between the $-\text{SO}_3\text{H}$ functionalized imidazolium dication to see the effect of cation structure on the resultant POM-based hybrids (DILPOMs) (**Scheme-4.1**), to tune the solubility properties as well as the acidity of hybrid materials. [DILPOM]-1 as 2-methyl-1-(3-(2-methyl-3-sulfo-1H-imidazol-3-ium-1-yl)propyl)-3-sulfo-1H-imidazol-3-ium phosphomolybdate, [DILPOM]-2 as 2-methyl-1-(4-(2-methyl-3-sulfo-1H-imidazol-3-ium-1-yl)butyl)-3-sulfo-1H-imidazol-3-ium phosphomolybdate, [DILPOM]-3 as 2-methyl-1-(12-(2-methyl-3-sulfo-1H-imidazol-3-ium-1-yl)dodecyl)-3-sulfo-1H-imidazol-3-ium phosphomolybdate are the three synthesized dicationic IL-POM hybrids reported in here. Their catalytic activities were investigated for one-pot synthesis of 3-substituted indoles involving Michael-like addition of indole to chalcones obtained from *in situ* Claisen Schmidt condensation of acetophenone with aromatic aldehydes.



Scheme 4.1: Synthesis of [DILPOM]-1/2/3 hybrids.

4.2 Results and discussion

The synthesis was completed according to the reaction **Scheme 4.1** and the solid materials synthesized were subjected to different analytical techniques for characterization.

4.2.1 FT-IR analysis

The FT-IR spectroscopic analysis of the parent 12-molybdophosphoric acid ($\text{H}_3\text{PMO}_{12}\text{O}_{40}\cdot n\text{H}_2\text{O}$ or PMA) along with the hybrids [DILPOM]-1, [DILPOM]-2, [DILPOM]-3 are represented in **Fig. 4.1** to their possible vibrations of different functional groups and bonds. The typical characteristic FTIR bands of the PMA are seen to have retained its fingerprint region in the hybrids as well at 1065, 956, 870 and 790 cm^{-1} [58]. Peak at 1628 cm^{-1} in PMA is assigned to bending vibrations of water molecules in the secondary structures of the Keggin unit. These bending mode frequencies of water molecule is observed to be shifted to 1600 cm^{-1} and 1612 cm^{-1} for the [DILPOM]-1 and [DILPOM]-2 respectively due to weaker extent of hydrogen bond interactions with bound water molecules in contrast to the [DILPOM]-3 at 1635 cm^{-1} . These results infer presence of a stronger intermolecular hydrogen bond interactions between the [DILPOM]-3 hybrid and the bound water molecules [59]. The obtained data also suggests presence of more intramolecular hydrogen bond interactions within the $-\text{SO}_3\text{H}$ groups of cations and polyoxometalate anion in [DILPOM]-1 and [DILPOM]-2 compared to [DILPOM]-3.

Imidazole ring stretching peaks are observed at 1520 cm^{-1} for all the hybrids. Weak intensity peak at a range of 1426-1449 cm^{-1} can be assigned to the C-C in ring stretch vibration. The asymmetric S-O stretch was observed in the range 1212-1269 cm^{-1} whereas symmetric S-O stretch at range of 1050-1065 cm^{-1} is observed to have overlapped with the characteristic P-O stretch at 1065 cm^{-1} . The N-S vibration frequency band has been observed to overlap with the characteristic vibrational frequency of polyoxometalate at around the range of 847-879 cm^{-1} . Peaks observed at around 2918, 2923, 2929, 2926, 2850 3154 and 3160 cm^{-1} are assigned to imidazole ring (C-H) and aliphatic (C-H) stretching vibrations of the alkyl bridge. The connecting alkyl spacer groups between the imidazole rings as well as the methyl groups at 2 position of the imidazole showed C-H rocking (1350-1392 cm^{-1}) along with C-H bending (1450-1470 cm^{-1}) in the respective IR spectra of the IL- POMs [60].

Peaks observed within 3300-3500 cm^{-1} range in the hybrids indicates presence of -OH of sulfonic groups as well as bound water molecules in the rigid framework of phosphomolybdate anion [61].

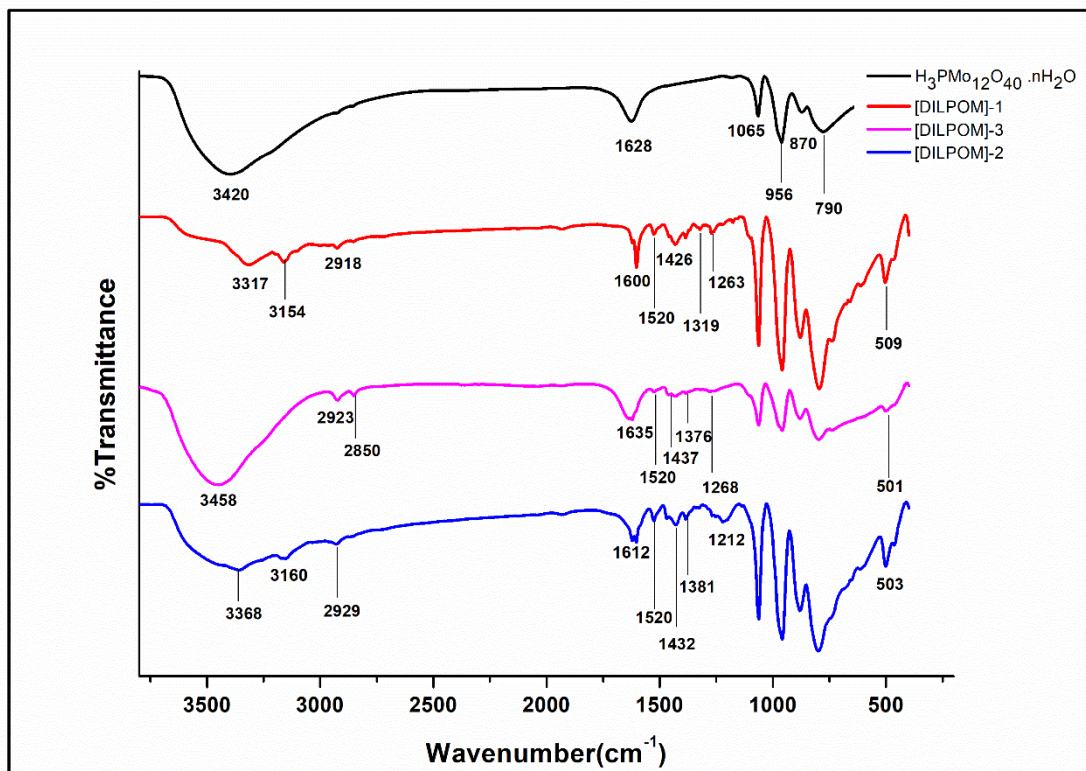


Fig. 4.1: FT-IR spectra of $\text{H}_3\text{PMO}_{12}\text{O}_{40}\cdot n\text{H}_2\text{O}$, [DILPOM]-1, [DILPOM]-2, [DILPOM]-3.

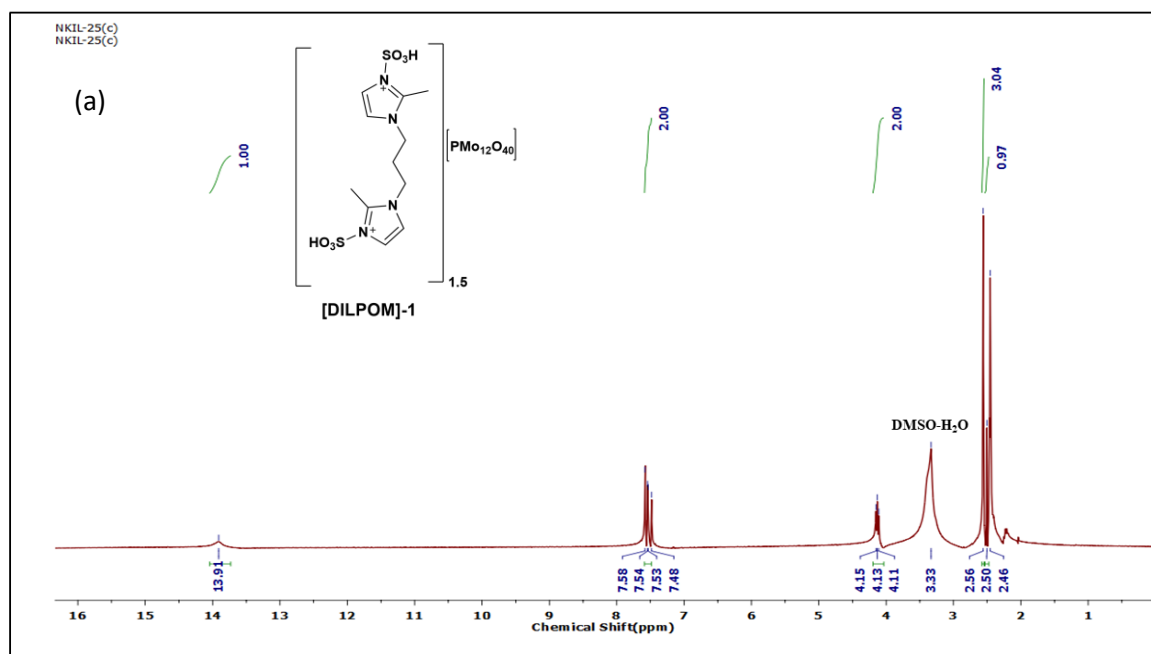
4.2.2 NMR analysis

The ^1H , ^{13}C and ^{31}P NMR spectra of the dicationic IL-POM hybrids in $\text{DMSO-}d_6$ depict their formation in **Fig. 4.2-4.4 (a, b, c)** respectively with different lengths of bridging methylene groups, ([DILPOM]-1, [DILPOM]-2, [DILPOM]-3).

For the [DILPOM]-1, ^1H NMR spectrum displayed one broad peak of two $-\text{SO}_3\text{H}$ protons at 13.91 ppm, multiplet of 4 protons of the two imidazole rings at 7.58-7.48 ppm. A triplet at 4.15-4.11 ppm for 4 protons and another singlet at 2.46 ppm for 2 protons of the propyl chain indicates incorporation of propyl chain between two imidazolium rings. A singlet at 2.56 ppm for 6 protons is observed for 6 methyl protons of the imidazole ring. The ^{13}C NMR showed 6 peaks at δ values of 144.77, 122.12, 118.71, 44.48, 29.31, 10.85 ppm. For the [DILPOM]-2, the ^1H NMR spectrum displayed one broad singlet peak of two $-\text{SO}_3\text{H}$

protons at 13.85 ppm, multiplet of 4 protons of the two imidazole rings at 7.61-7.45 ppm. One singlet at 2.46 ppm for 6 protons indicates presence of $-\text{CH}_3$ group at 2 positions of both the imidazole. A broad singlet at 4.10 ppm for 4 protons and another singlet at 1.75 ppm for another 4 protons indicates incorporation of butyl chain between two imidazolium rings. Similarly, the ^{13}C NMR of [DILPOM]-2, expressed 3 peaks at δ values of 119.27, 100.03 and 11.71. The ^1H NMR and ^{13}C NMR peaks for [DILPOM]-3, were displayed as follows: ^1H NMR (400 MHz, $\text{DMSO-}d_6$) δ (ppm): 13.84 (s, 2H), 7.59-7.45 (m, 4H), 4.01 (s, 4H), 2.43 (s, 6H), 1.66 (s, 4H), 1.18 (s, 16H); ^{13}C NMR (100 MHz, $\text{DMSO-}d_6$) δ (ppm): 144.25, 122.39, 118.56, 119.17, 29.38, 10.81.

The ^{31}P NMR, signal of these POM-IL hybrids **Fig. 4.4(a, b, c)** shifted towards up field region with lowering of chemical shift values as compared to the pure phosphomolybdic acid, **Fig 4.4d**. This can be accounted for existence of dynamic hydration environment nearby heteropoly anions of the IL-POM hybrids [62].



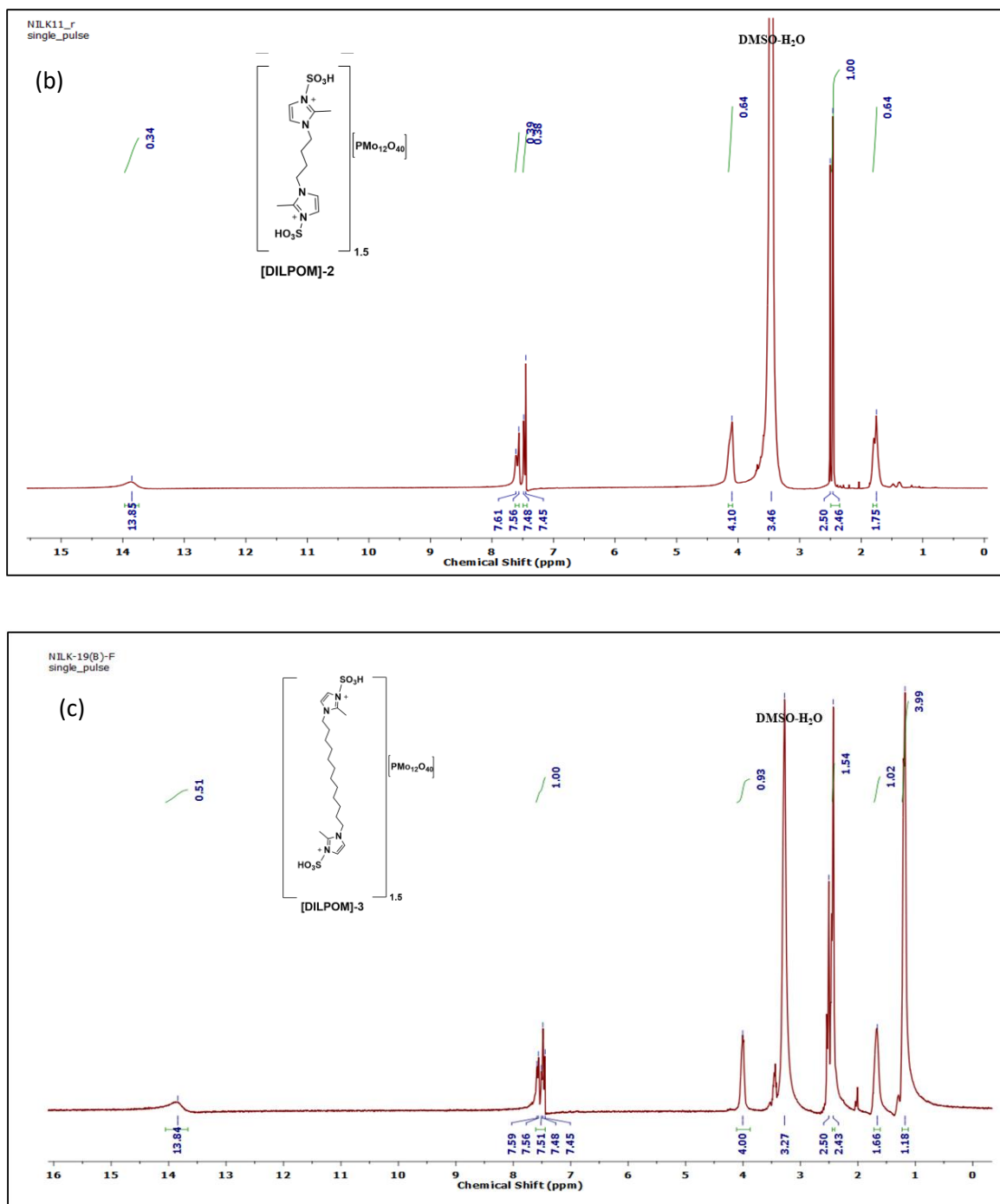
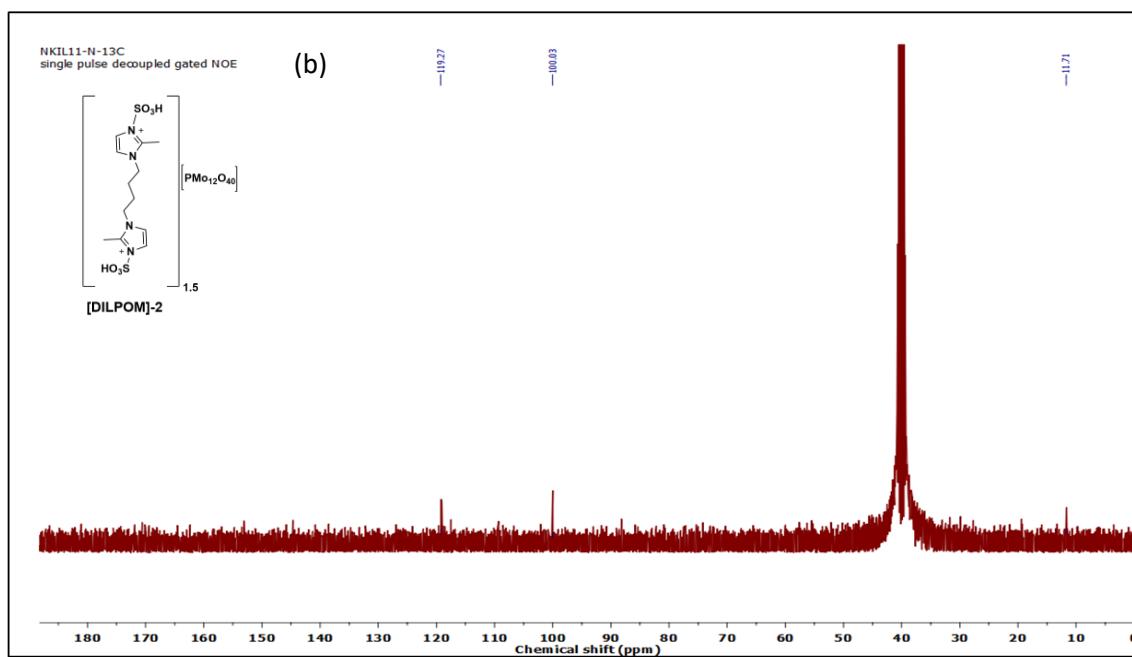
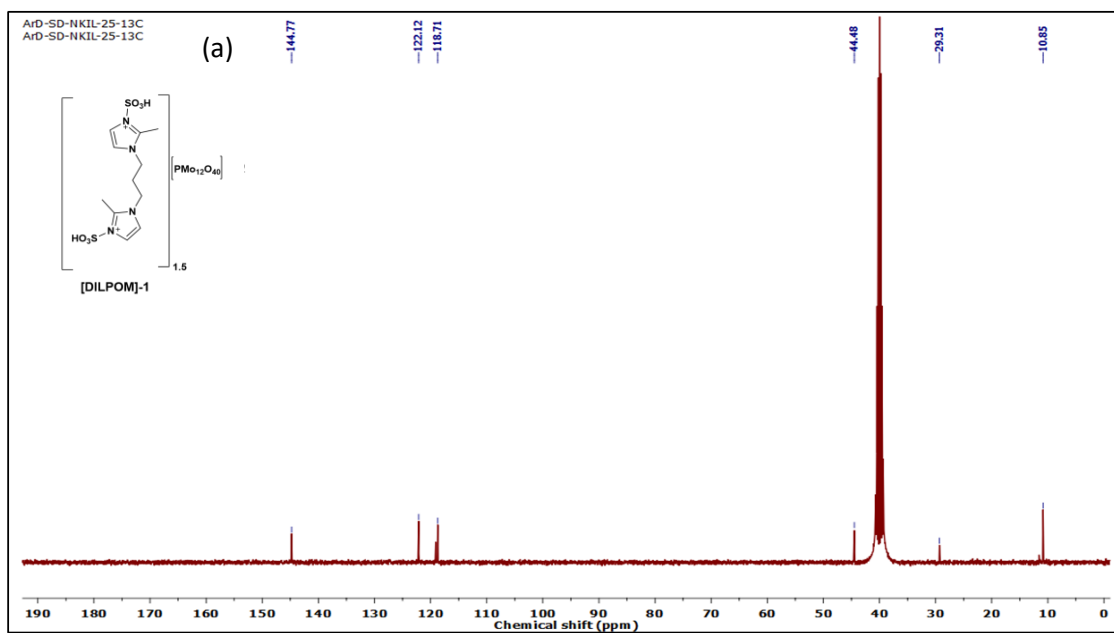


Fig. 4.2: (a) ^1H NMR of [DILPOM]-1, (b) ^1H NMR of [DILPOM]-2, (c) ^1H NMR of [DILPOM]-3



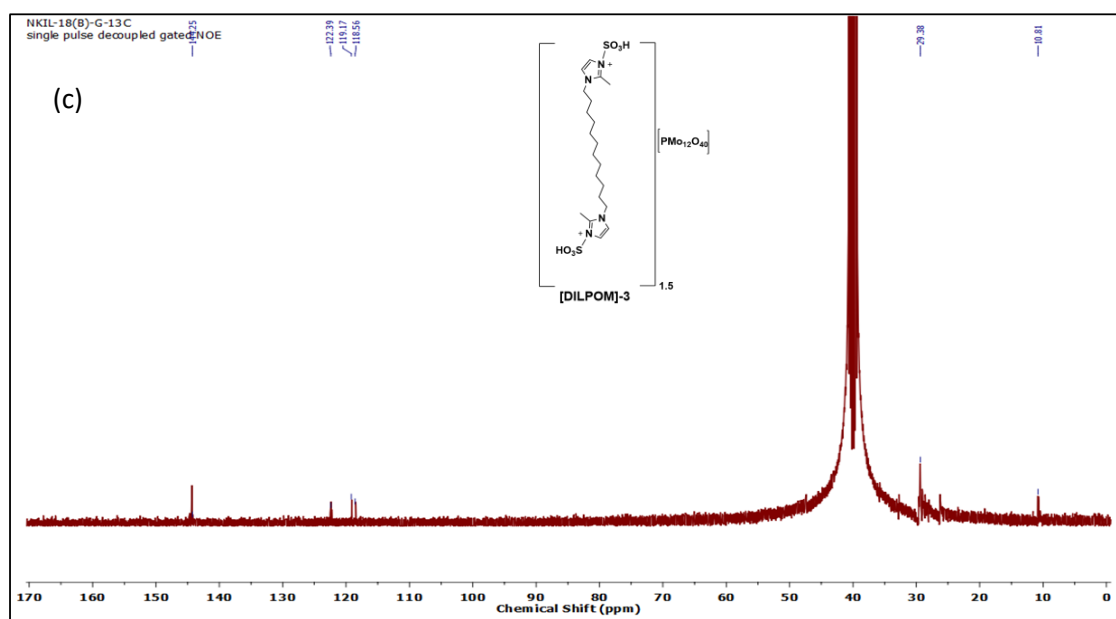
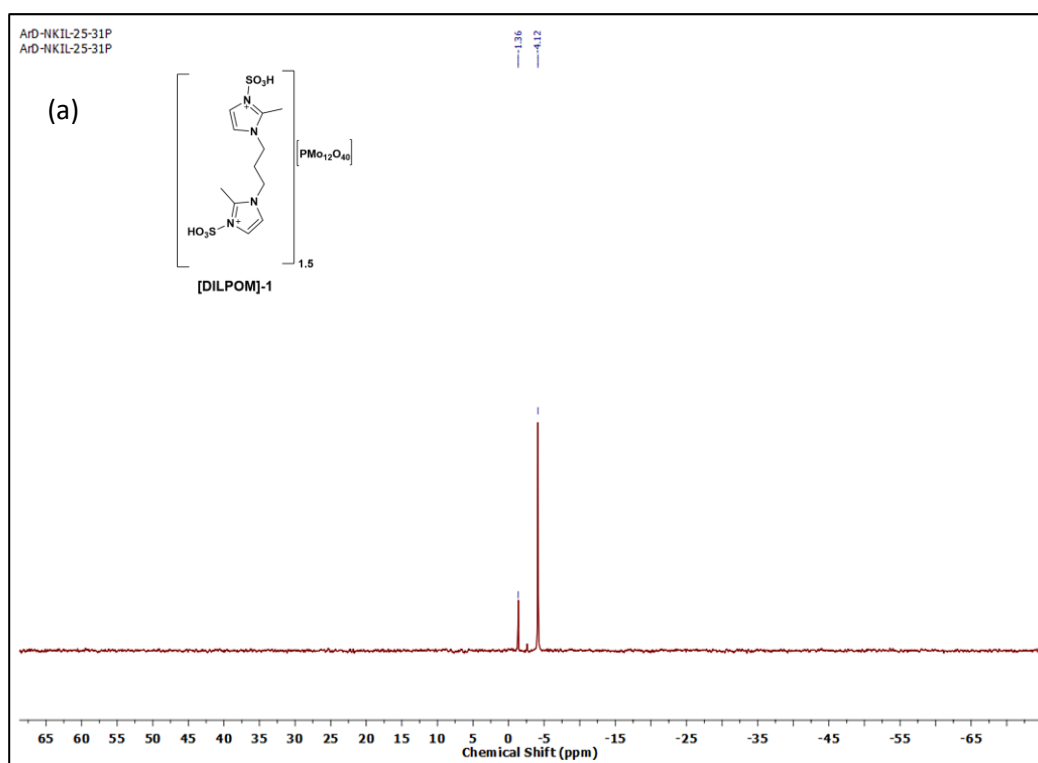
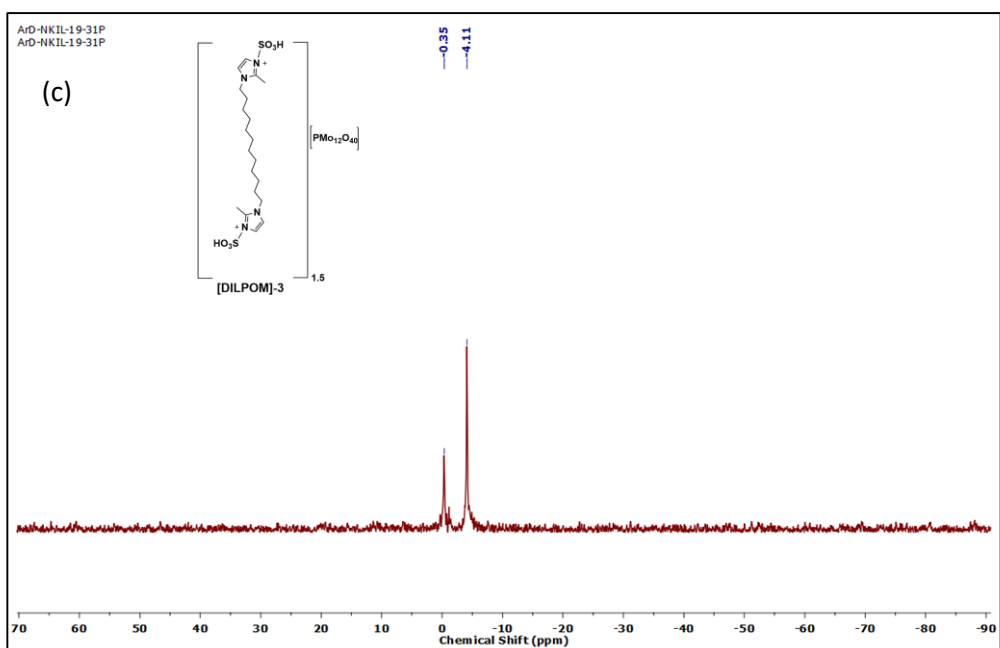
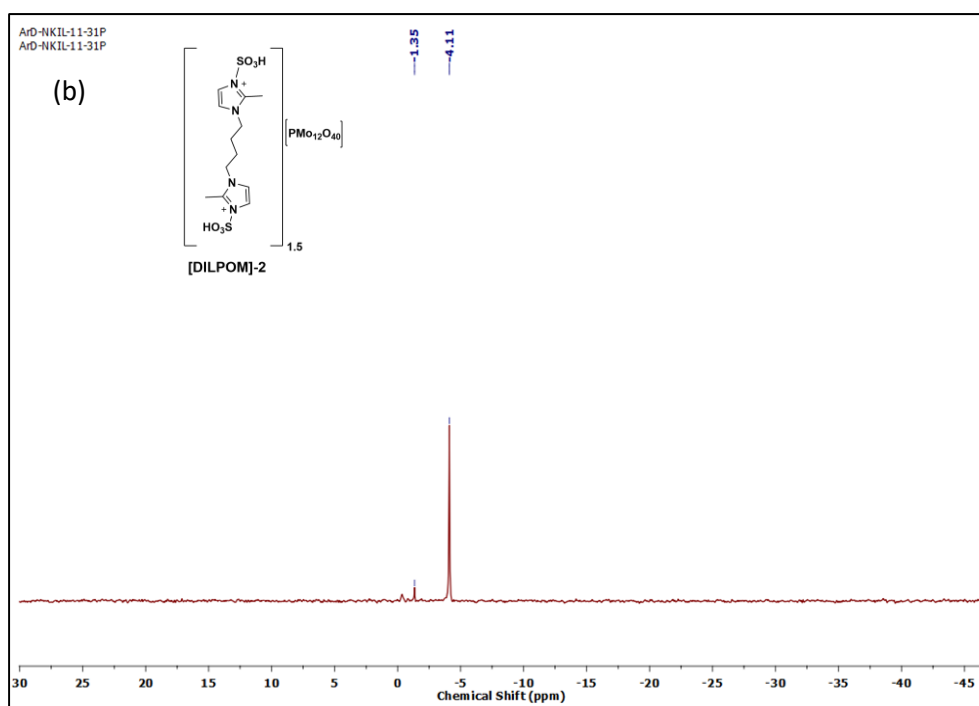


Fig. 4.3: (a) ^{13}C NMR of [DILPOM]-1, (b) ^{13}C NMR of [DILPOM]-2, (c) ^{13}C NMR of [DILPOM]-3.





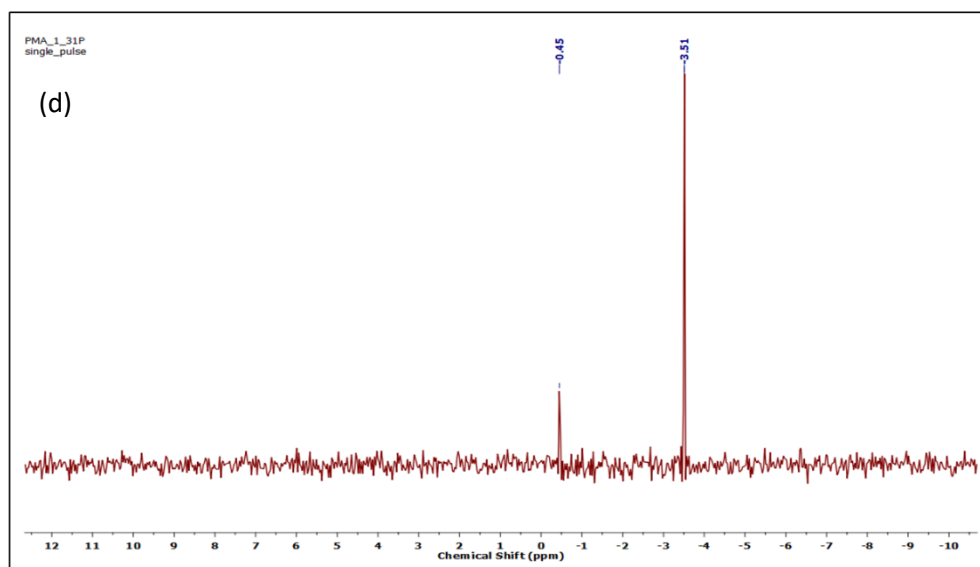


Fig. 4.4: (a) ^{31}P NMR of [DILPOM]-1, (b) ^{31}P NMR of [DILPOM]-2, (c) ^{31}P NMR of [DILPOM]-3 (d) ^{31}P NMR of $\text{H}_3\text{PMO}_{12}\text{O}_{40}\cdot n\text{H}_2\text{O}$.

4.2.3 Elemental analysis

The CHN analysis data of the three synthesized hybrids are presented as follows: [DILPOM]-1, calculated: C 8.37%, H 1.14%, N 3.55%, found: C 8.23% H 1.24% N 3.12%; [DILPOM]-2, calculated: C 9.05%, H 1.25%, N 3.52%, found: C 9.28% H 1.45% N 3.75%; [DILPOM]-3, calculated: C 10.19%, H 2.12%, N 3.18%, found: C 11.12% H 2.98% N 3.19%.

4.2.4 TGA

Thermogravimetric analysis (TGA) showed absence of physisorbed water (**Fig. 4.5**), for the three hybrids [DILPOM]-1/2/3 as compared to the physisorbed water present in $\text{H}_3\text{PMO}_{12}\text{O}_{40}\cdot n\text{H}_2\text{O}$ where $n = 25$, as well as their respective parent dicationic chloride ionic liquids namely [DIL-1] $\cdot 16\text{H}_2\text{O}$ / [DIL-2] $\cdot 25\text{H}_2\text{O}$ / [DIL-3] $\cdot 21\text{H}_2\text{O}$. Among the three parent chloride DILs, shorter methylene bridged imidazolium IL i.e. DIL-1 displayed greater thermal stability by showing stepwise degradations at 100 °C and around 250 °C that can be expected for removal of the physisorbed water and $-\text{SO}_3\text{H}$ groups of the imidazolium units respectively. In contrast, the other two chloride ionic liquids with 4 and 12 carbon numbers of methylene bridging chains expressed degradation with highest

amount of physisorbed water (approx. 50% and 40% weight loss) for DIL-2 and DIL-3 ionic liquids respectively.

The TGA plots of [DILPOM]-1 hybrids displayed their thermal stability till 350 °C contrary to 300 °C for the [DILPOM]-3 hybrid and [DILPOM]-2 without loss of any physisorbed water up to 100 °C. The absence of physisorbed water in the IL-POM hybrids indicates that the water molecules present in the scaffold of pure 12-molybdophosphoric acid are now occupied by dicationic disulphonic methylene bridged imidazolium moiety. Thus extensive intra and intermolecular hydrogen bond interactions, electrostatic interactions resulted in hydrophobic nature of hybrids. These changes increases shelf life of the hybrids due to less moisture sensitivity. Above 300 °C, the organic cation part starts degrading i.e. the thermal energy breaks secondary interactions like strong hydrogen bond interactions, ion-dipole interactions in these hybrids which are responsible for holding the large dicationic disulfonic methylene bridged imidazolium moiety and the polyoxometalate anion together.

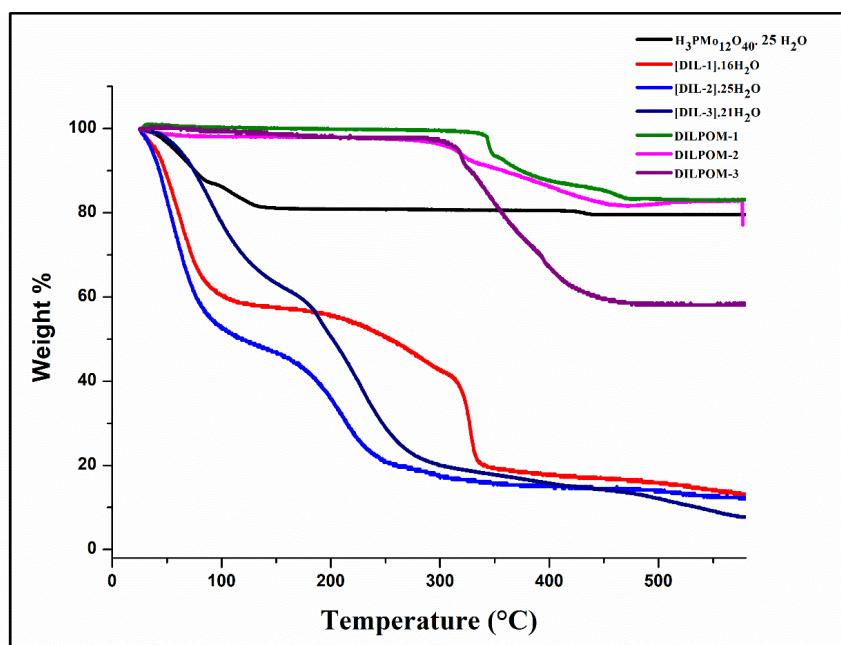


Fig. 4.5: TGA graphs of [DILPOM]-1, [DILPOM]-2, [DILPOM]-3, [DIL-1]·16H₂O, [DIL-2]·25H₂O, [DIL-3]·21H₂O and H₃PMo₁₂O₄₀·25H₂O.

4.2.5 Powder X-Ray Diffraction analysis

The powder XRD patterns of both the pure 12-molybdophosphoric acid along with [DILPOM]-1/2/3 hybrid samples are represented in **Fig. 4.6 (a)/(b)/(c)/(d)** respectively.

Typical high intensity sharp diffraction peak for $\text{H}_3\text{PMo}_{12}\text{O}_{40}\cdot n\text{H}_2\text{O}$ is observed at $2\Theta = 26.79^\circ$ [Fig. 4.6(a)]. In case of [DILPOM]-1, the intensity of all the peaks decreased although the characteristic high intensity peak for Keggin anion shifted to $2\Theta = 26.12^\circ$. In [DILPOM]-1, broadening of the peaks was observed, this might have occurred due to organization of the large organic cation over the spaces within polyoxoanion involving self assembly of the $[\text{PMo}_{12}\text{O}_{40}]^{3-}$ anions and the organic cations via electrostatic force, hydrogen bond interactions etc. replacing the acidic protons along with physisorbed water. This type of arrangement in the hybrids bring changes in the crystal structure of the pure polyoxometalate and these changes can be seen with broadening of peaks which may be a result of loss of crystallinity and turning into amorphous material. Similar results were also observed in case of [DILPOM]-2 hybrid. For the [DILPOM]-3, the sharp peaks totally vanished with increased broadening and this result suggests that the secondary structure of polyoxomolybdate has been completely modified by this large cation with 12 carbon number methylene bridged imidazolium dication. Due to presence of the long alkyl chain in [DILPOM]-3, the hydrophobic alkyl groups of the organic cations repel the H_2O molecules inside the POM which leads to compact arrangement in the POM. Thus, introduction of large cation with long alkyl chain deviates the plane spacing in the POM structure thus resulting in increased broadening. Also, the length of the alkyl bridge in dications modifies the electrostatic interaction, and hence the packing between the charged sub-units of these hybrids also modifies. The structural transformations of the hybrids with varied cation sizes are detected by powder X-ray diffraction. It is noteworthy that the broadening of peak is a characteristic of amorphous materials and here it can be observed that as the methylene chain lengths in dication increases the sharp crystalline peak disappeared in [DILPOM]s. It can be said that increase in the number of carbons in the alkyl chains brings the structural transformation in the whole cation-anion pair [60].

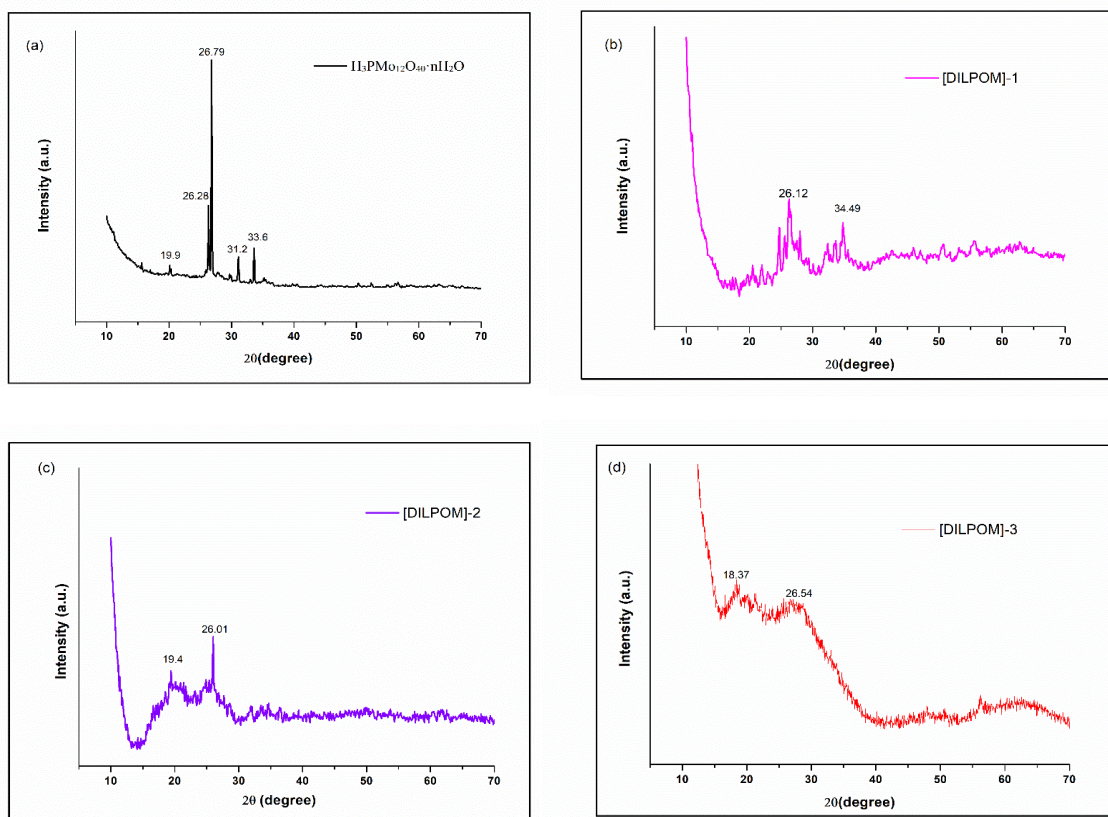


Fig. 4.6: Powder XRD analysis patterns of (a) $\text{H}_3\text{PMo}_{12}\text{O}_{40}\cdot n\text{H}_2\text{O}$, (b) [DILPOM]-1, (c) [DILPOM]-2, (d) [DILPOM]-3.

4.2.6 Raman analysis

Raman spectra of the hybrids in **Fig. 4.7** (a), (b), (c) showed resemblance of characteristic bands of the anions $[\text{PMo}_{12}\text{O}_{40}]^{3-}$ observed from Bridgeman's assignments [58,63]. Precisely, the $[\text{PMo}_{12}\text{O}_{40}]^{3-}$ anion with α -Keggin structure is an assembly of a $[\text{PO}_4]$ tetrahedron and $[\text{MoO}_6]$ octahedra units [58]. Four C_{3v} $[\text{Mo}_3\text{O}_{13}]$ groups are formed by edge sharing of $[\text{MoO}_6]$ octahedral units. 4 types of Mo-O bonds are present in the 12-molybdophosphoric acid structure. The terminal Mo-O_t bond is the bond that connects the metal to the centre of the distorted C_s octahedra. 3 groups of $[\text{MoO}_6]$ and the only $[\text{PO}_4]$ unit are connected via the four-coordinate oxygen atoms termed as M-O_{4c} bonds. The remaining two types of the two coordinate oxygen atoms are Mo-O_{2c1} and Mo-O_{2c2}. Mo-O_{2c1} corresponds to connecting the $[\text{MoO}_6]$ octahedra with the $[\text{Mo}_3\text{O}_{13}]$ units while the Mo-O_{2c2} bonds links the $[\text{Mo}_3\text{O}_{13}]$ units together. Sharp peaks at 990, 998, 1001 cm^{-1} for the [DILPOM]-1, [DILPOM]-2, [DILPOM]-3 respectively are observed due to symmetric stretch Mo-O_t bonds. Peaks at 885 and 892 cm^{-1} for the [DILPOM]-2 and 3 respectively are designated for asymmetric stretch of Mo-O_{2c2}-Mo bonds. Combined stretching and

bending vibrations of Mo-O_{2c1}-Mo could be attributed to medium intensity broad shoulder at 648 cm⁻¹ in case of the and [DILPOM]-1 and 605 cm⁻¹ for the [DILPOM]-2 and 589 cm⁻¹ for [DILPOM]-3. Polarized Raman bands of the [DILPOM]-1 and [DILPOM]-2 at 274 cm⁻¹ and 241 cm⁻¹ respectively can be attributed to symmetric stretch of the Mo-O_{4c} bonds [58,63]. Few bands are not allocated as they belong to modes that involve complex motions related to the polyoxometalate scaffold.

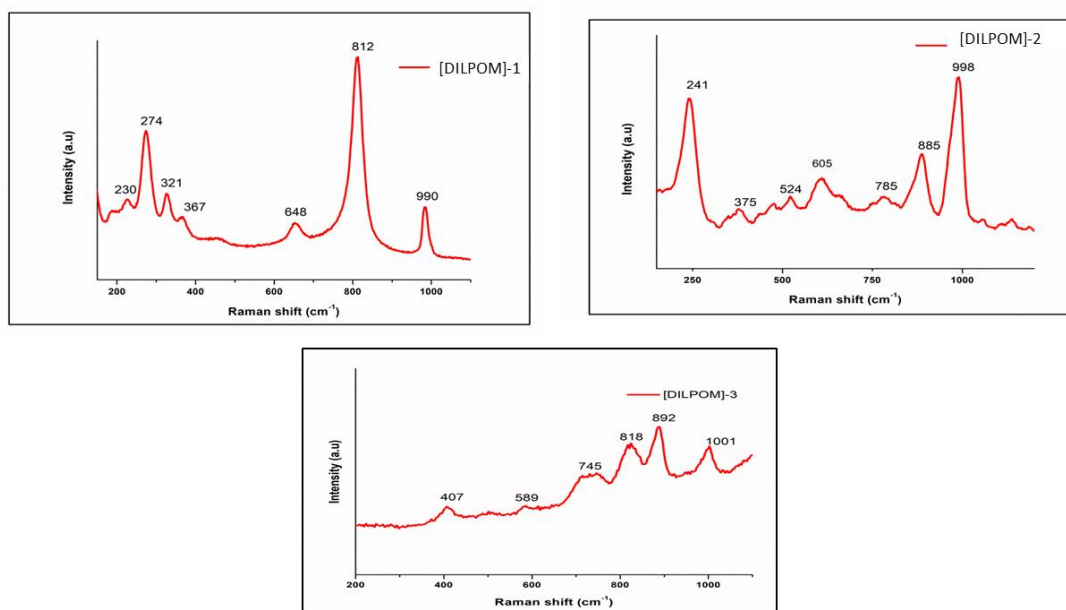


Fig. 4.7: Raman spectra of (a) [DILPOM]-1, (b) [DILPOM]-2, (c) [DILPOM]-3.

4.2.7 UV-Vis diffuse reflectance spectroscopy analysis

The UV-Vis diffuse reflectance spectra of the [DILPOM]-1/2/3 hybrids against H₃PMo₁₂O₄₀·nH₂O are represented in **Fig. 4.8 (a), (b) and (c)**. It is well known that 12-molybdophosphoric acid in their non reduced form shows characteristic bands for oxygen to metal charge transfer. In case of [DILPOM]-1/2/3, on irradiation with UV light, electrons are mainly excited from oxygen 2p orbitals to the phosphorus 3d orbitals of the [PMo₁₂O₄₀]³⁻. These transitions are likely to be observed below 250 nm in these hybrids. A high intensity peak towards higher wavelength at 458 nm correspond to transition from oxygen to metal (O²⁻ to Mo⁶⁺) within Keggin anion in 12-molybdophosphoric acid. The highly intensified peak of PMo₁₂O₄₀³⁻ in 12-molybdophosphoric acid at 458 nm is shifted below 400 nm in [DILPOM]-1/2/3 hybrids. As in the Raman analysis description, it is already mentioned that three types of oxygen are present in 12-molybdophosphoric acid i.e., bridge, corner, and terminal oxygen in the scaffold. Therefore, there is possibility of

appearance of more than one absorption band below 400 nm in the hybrids that corresponds to transitions within the oxygen and metal of the anion as well as from oxygen of cation to metal of the Keggin anion. The shifting of peak in the [DILPOM]-1/2/3 compared to 12-molybdophosphoric acid presents a strong indication for intermolecular interaction of the dications with the $[\text{PMo}_{12}\text{O}_{40}]^{3-}$ anions [64].

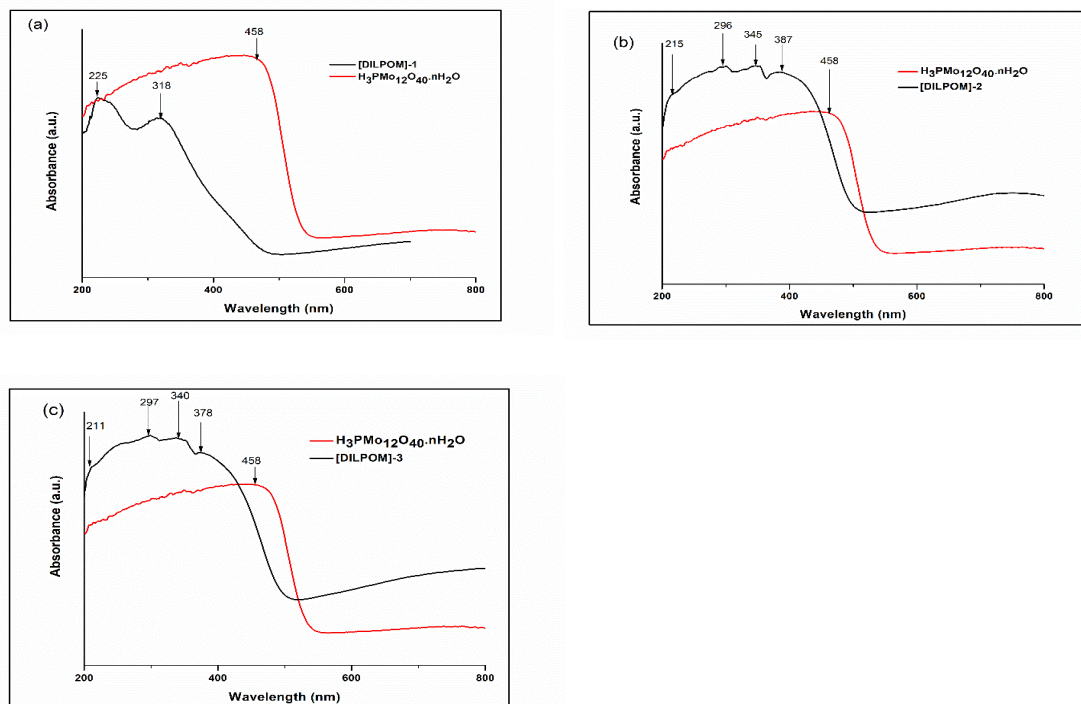


Fig. 4.8: UV-Vis DRS spectra of (a) $\text{H}_3\text{PMo}_{12}\text{O}_{40}\cdot n\text{H}_2\text{O}$ vs [DILPOM]-1, (b) $\text{H}_3\text{PMo}_{12}\text{O}_{40}\cdot n\text{H}_2\text{O}$ vs [DILPOM]-2 (c) $\text{H}_3\text{PMo}_{12}\text{O}_{40}\cdot n\text{H}_2\text{O}$ vs [DILPOM]-3.

4.2.8 SEM analysis

The surface morphology images of the 12-molybdophosphoric acid (observed at 100X magnification) and also the hybrid salts [DILPOM]-1/ 2/ 3 (observed above 1000X magnification) are represented in **Fig. 4.9 (a)/(b)/(c)/(d)** respectively. It is observed that incorporation of the imidazolium cation to the polyoxometalate anion in these hybrids leads to modification of surface morphology with agglomerated small particles observed in surface compared to the crystalline 12-molybdophosphoric acid. The absence of physisorbed water as observed from the TGA plots (**Fig. 4.5**) may be favorable for formation of intramolecular hydrogen bond interactions among the molecules of IL-POM hybrids *via* sulfonic groups. These electrostatic interactions can be attributed for compactness in the [DILPOM]s structures. The reason behind this compactness may be a

result of van der Waals forces which come into play with incorporation of methylene bridging spacers of different lengths between the imidazolium moities [65].

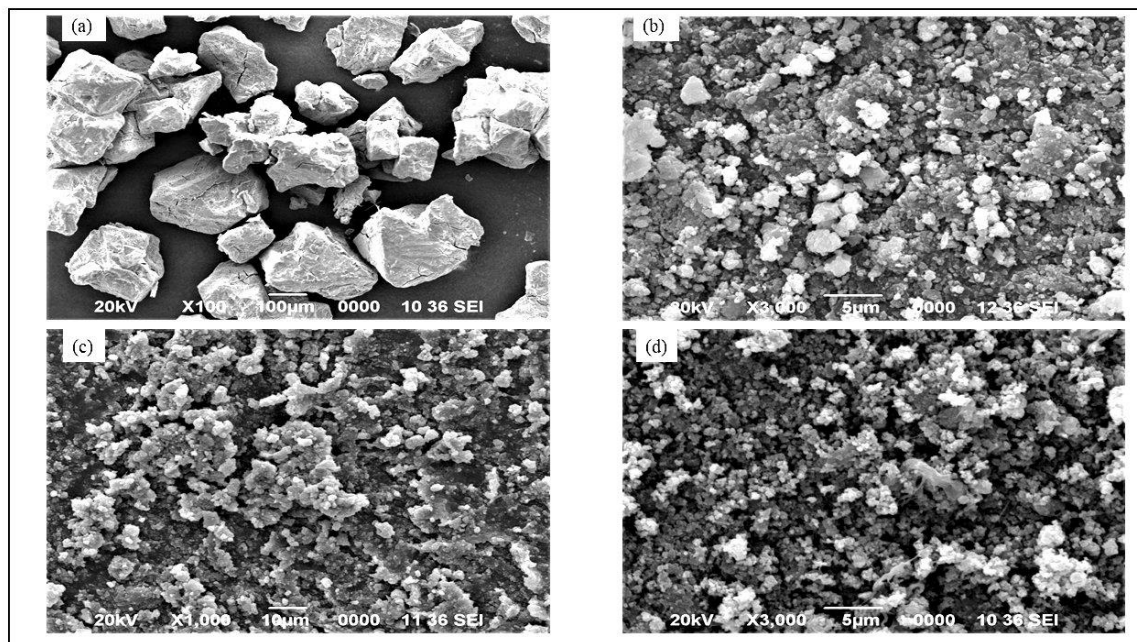


Fig. 4.9: SEM images of (a) $H_3PMO_{12}O_{40} \cdot nH_2O$, (b) [DILPOM]-1, (c) [DILPOM]-2, (d) [DILPOM]-3.

4.2.9 EDX analysis

Energy Dispersive X-ray (EDX) spectra of the [DILPOM]-1, [DILPOM]-2, [DILPOM]-3 in **Fig. 4.10 (a), (b), (c)** confirmed presence of C, N, O, P, Mo and S as the constituent elements of the hybrid compounds.

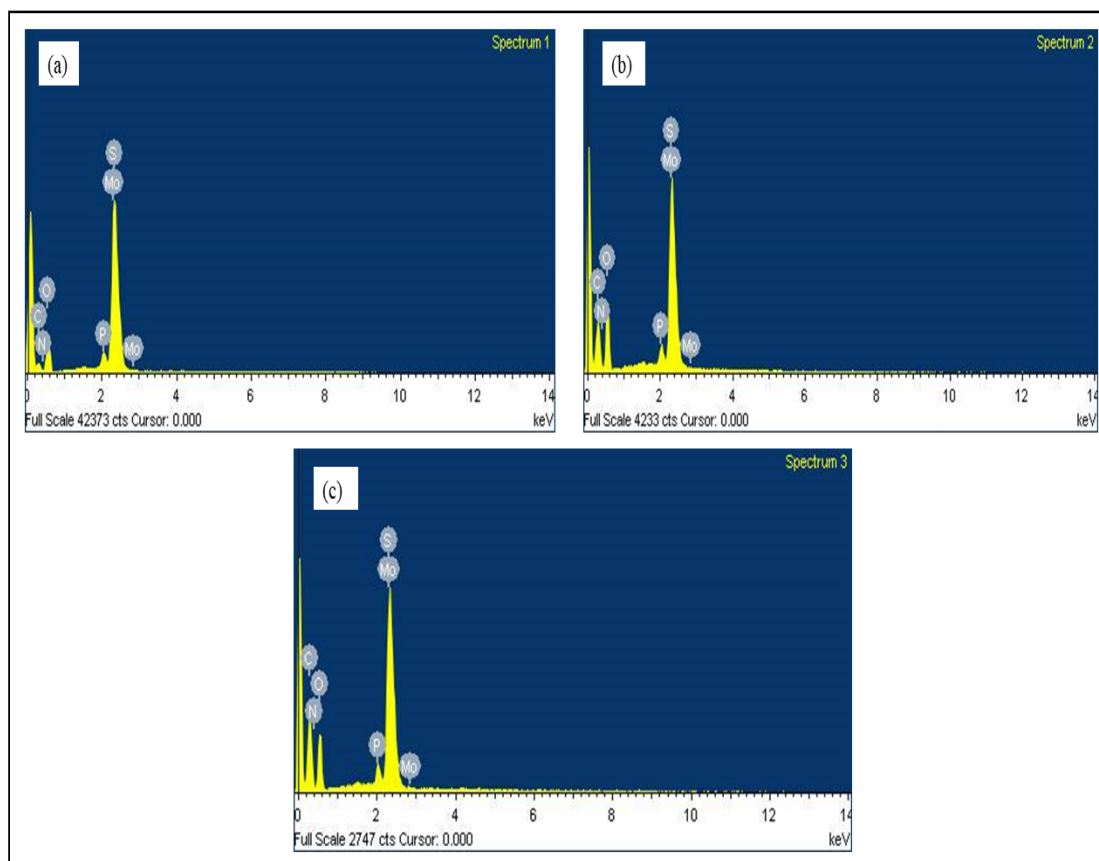


Fig. 4.10: EDX patterns of (a) [DILPOM]-1, (b) [DILPOM]-2, (c) [DILPOM]-3.

4.2.10 Determination of acidic sites in the hybrids

The existence of Brønsted-Lewis acidic sites in these POM-IL hybrids were identified via FT-IR spectra after complexation of the hybrids with pyridine as probe molecule as included in **Fig. 4.11**. In this Fig., it is seen that ring bending vibrations of pyridine can be found at 1590 cm^{-1} and 1440 cm^{-1} . The co-ordination of pyridine probe molecule with the Lewis acidic sites of hybrids displayed another strong peak at 1484 cm^{-1} . Likewise, the hybrids also showed one new peak around $1538\text{-}1540\text{ cm}^{-1}$ that can be assigned as an outcome of interactions of the pyridine with the Brønsted acidic sites forming pyridinium ion [66]. It was noteworthy that the intensity of peak at 1540 cm^{-1} in [DILPOM]-3 is higher than the other two hybrids. This result indicates presence of a greater number of free $\text{-SO}_3\text{H}$ Brønsted acidic sites in case of the [DILPOM]-3 due to decreasing number of intramolecular hydrogen bond interactions between the counterions in [DILPOM]-3 with increasing the length of methylene alkyl bridges. The FT-IR spectra interpretation of the IL-POMs provided in subsection **4.2.1** also justifies the outcomes found while determining their acidic sites. It was observed in subsection **4.2.1**, that the intermolecular hydrogen

bond interactions in [DILPOM]-3 is stronger than [DILPOM]-1 and [DILPOM]-2. However, the intramolecular hydrogen bond interactions were stronger in [DILPOM]-1 and [DILPOM]-2 compared to [DILPOM]-3. Thus, the acidity is reduced in [DILPOM]-1/2 compared to acidity in [DILPOM]-3, because of the effects of intramolecular hydrogen bonding [67]. The acidic sites present in the hybrids was used for acid catalysed solvent-free Michael-Like addition.

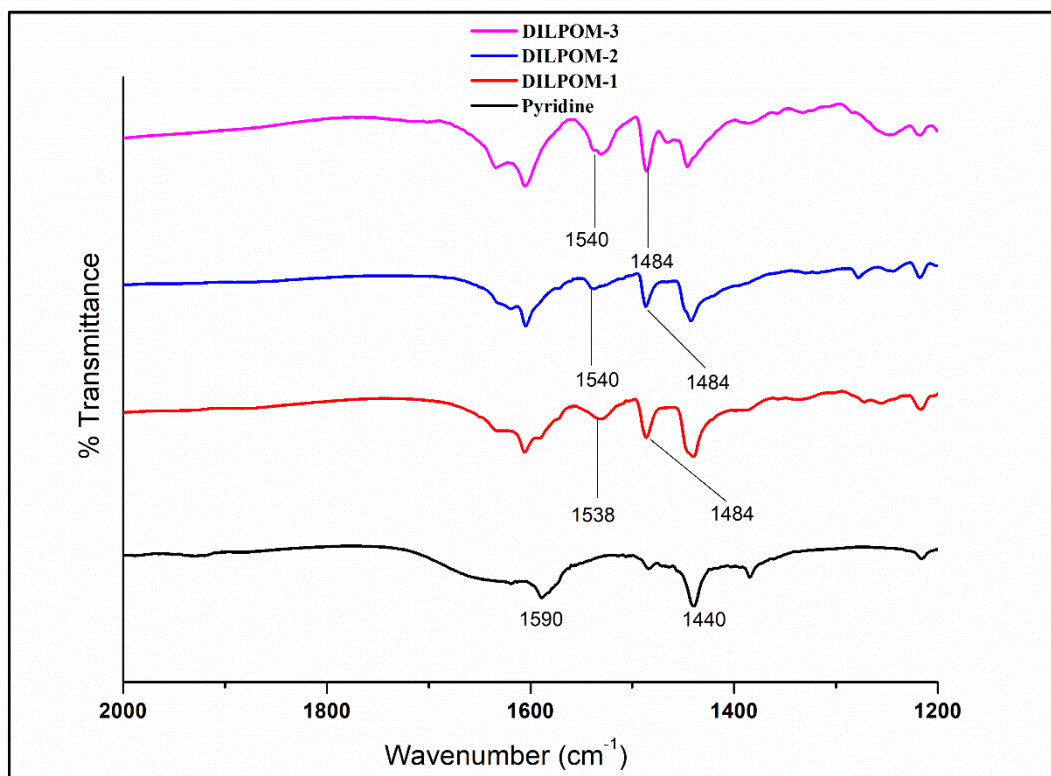


Fig. 4.11: FT-IR study for Brønsted- Lewis acidic sites of the POM-IL hybrids.

Another experimental analysis, NH₃-TPD was done for [DILPOM]-1/2/3 (**Fig. 4.12**) to understand the distribution of acid strength. Above 300 °C, there was stepwise degradation of -SO₃H groups in [DILPOM]-1/2/3 as observed from the TGA analysis graph, **Fig. 4.5**. From the graphs given in **Fig. 4.12**, it can be observed that below 300 °C, there were peaks present for acidic sites for all the three hybrids. With weaker intramolecular interactions between the ion pairs with increase in methylene chain lengths, the number of freely available -SO₃H sites increased.

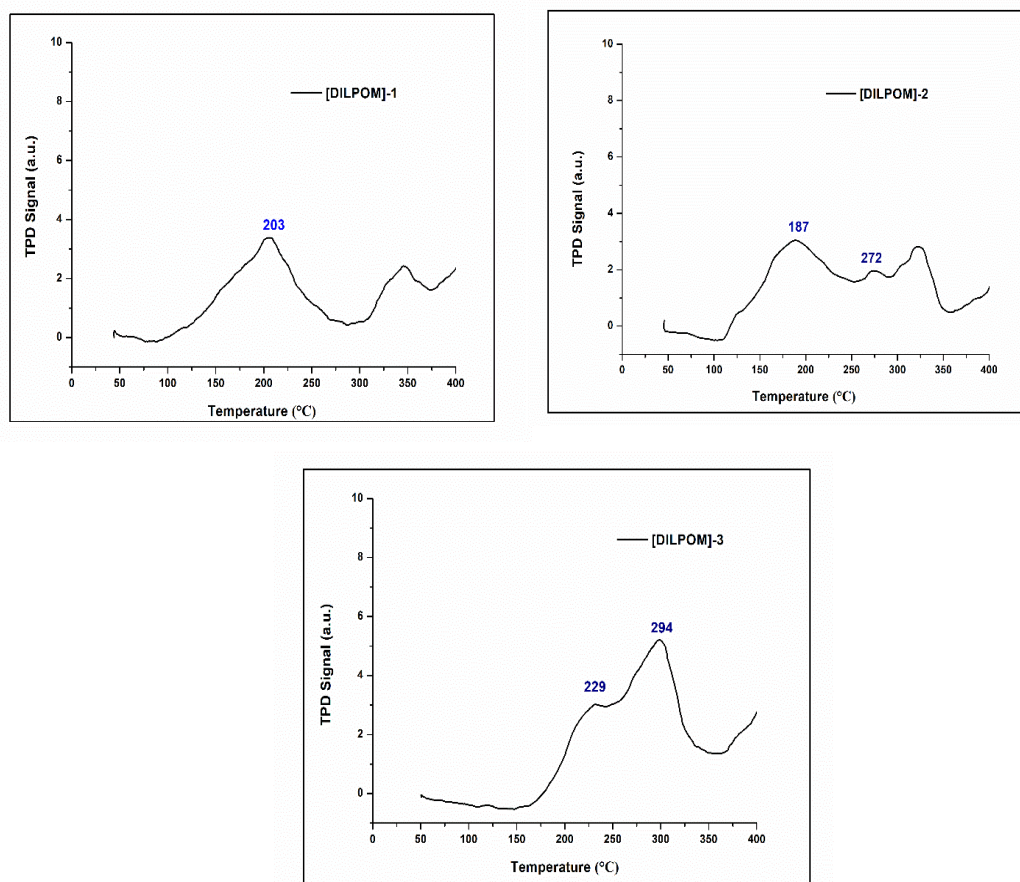
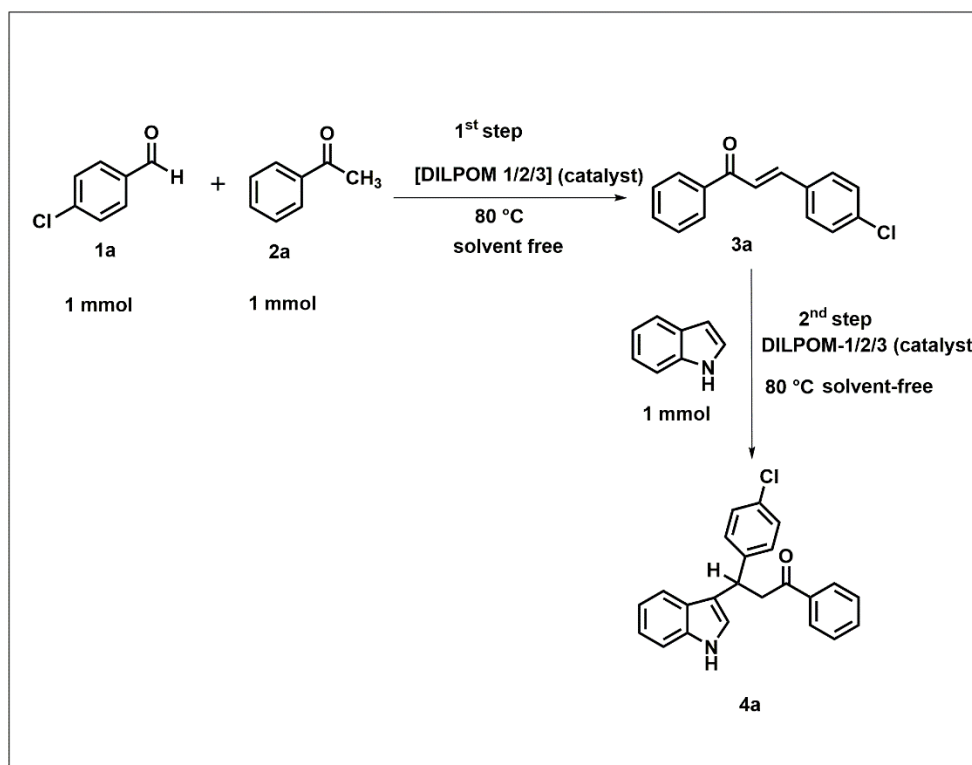


Fig. 4.12: NH₃-TPD graphs of [DILPOM]-1,2,3.

4.3 Catalytic activity study

The catalytic activity of newly developed acidic di-cationic imidazolium polyoxometalate hybrids salts [DILPOM]-1/2/3 were evaluated as acid catalyst for two-step synthesis of 3-substituted indoles through sequential Claisen-Schmidt condensation followed by Michael-like addition reaction (**Scheme 4.2**). For this purpose, initially 4-chlorobenzaldehyde (1 mmol) is reacted with acetophenone (1 mmol) in presence of 10 mol% of [DILPOM]-1/2/3 for synthesis of chalcones (1st step) followed by addition of indole (1mmol) (2nd step). Both the steps of the reaction were studied to optimize the reaction conditions for the synthesis of chalcones and 3-substituted indole derivatives.



Scheme 4.2: Model reaction for optimization of sequential Claisen-Schmidt condensation followed by Michael-Like addition.

4.3.1 Screening of POM-IL hybrid catalysts for preparation of model Claisen-Schmidt product (3a) in step-I

Initially, the screening of catalytic activities of [DILPOM]-1/2/3 were investigated for the model reaction by taking 1 mmol of the substrates (Scheme 2) in solvent-free conditions at 80 °C using 5 and 10 mol % of the hybrid catalysts (**Table 4.1**, entries 1-6) for the preparation of chalcone derivative **3a**. The results expressed higher catalytic activity for the [DILPOM]-3 hybrid with both the amounts (**Table 4.1**, entries 5 & 6) as compared to the other two hybrids (**Table 4.1**, entries 1-4) within 1 hour reaction time at 80 °C. Increasing amount of the catalyst produced excellent isolated yield of the product **3a** (96%) in case of 10 mol% the [DILPOM]-3 hybrid (**Table 4.1**, entry 6). The same reaction, under mechanochemical method showed very poor yield of product at room temperature (**Table 4.1**, entry 7). The reaction was also performed at a medium temperature of 60 °C with 10 mol % [DILPOM]-3. The reaction yielded 85% of chalcone (**3a**) in 1h however, only 58% of **4a** as major product in next 2 hours (**Table 4.1**, Entry 8). Since, the reaction is a solid-state reaction, so at temperatures of 80 °C or above, all the substrate melts, which resulted in uniform mixing of substrates and catalyst that helps the

reaction to work well. The model reaction was then subjected to solvent study in two solvents i.e., acetonitrile and water at 80 °C using 10 mol% of the [DILPOM]-1 and [DILPOM]-3 (**Table 4.1**, entries- 9, 10, 11). Both the catalysts were insoluble in these solvents. It was observed that the reaction with [DILPOM]-3 showed considerable yield in acetonitrile (**Table 4.1**, entry 11) while the yield using water as solvent was comparatively better but took longer hours. Due to longer methylene bridging chain of the [DILPOM]-3 catalyst, it showed better hydrophobic interactions towards the hydrophobic substrate molecules in water than the less hydrophobic [DILPOM]-1 catalyst, resulting higher yield of the **3a** (**Table 4.1**, entry 10) in water. However, the solvent free reaction condition provided us with highest yield of **3a** in shorter reaction time. So, it was decided to conduct the reaction in neat condition at 80 °C for *in situ* generation of the chalcone derivative (**3a**) as single product for subsequent Michael-like addition reaction with indole without separation of the hybrid catalyst.

Table 4.1: Optimization of reaction conditions for synthesis of 3-substituted indoles

Entry	Catalyst	mol %	Reaction Solvent	Temp. (1 st step)	Time (1 st step)	^[a] Yield % (3a)	Temp. (2 nd step)	Time (2 nd step)	^[b] Yield% (4a)
1	[DILPOM]-1	5	Solvent-free	80°C	1h	80	-	-	-
2	[DILPOM]-1	10	Solvent-free	80°C	1h	86	-	-	-
3	[DILPOM]-2	5	Solvent-free	80°C	1h	80	-	-	-
4	[DILPOM]-2	10	Solvent-free	80°C	1h	80	-	-	-
5	[DILPOM]-3	5	Solvent-free	80°C	1h	90	-	-	-
6	[DILPOM]-3	10	Solvent-free	80°C	1h	96	80°C	2h	80
7	[DILPOM]-3	5	Solvent-free	r.t	1h	>5	-	-	-
8	[DILPOM]-3	10	Solvent-free	60°C	1h	85	60°C	2h	58
9	[DILPOM]-1	10	Water	80°C	5h	72	-	-	-
10	[DILPOM]-3	10	Water	80°C	5h	80	-	-	-
11	[DILPOM]-3	10	Acetonitrile	80°C	5h	68	-	-	-
12	[DILPOM]-3	10	Solvent-free	80°C	1h	96	100°C	2h	75
13	[DILPOM]-3	10	Water	Reflux	5h	80	Reflux	8h	45
14	H ₃ PMO ₁₂ O ₄₀ ·25H ₂ O	10	Solvent-free	80°C	1h	52	-	-	-

^[a] Yield % = Calculated from isolated yield, Reaction conditions: 1mmol of each substrate.

^[b] Yield % = Calculated from isolated yield, Reaction conditions: 1mmol of indole added to the reaction pot after generation of **3a** in the 1st step.

At the same time, it is worth mentioning that the used catalyst [DILPOM]-3 can be utilized as easily recoverable heterogeneous catalyst because of its insoluble nature in any solvent additional to its good thermal stability after separation of the product **3a** for analytical purpose.

4.3.2 Optimization of reaction conditions for preparation of model Michael-like adduct (**4a**) in step 2

For optimization of the sequential Michael-like formation of adduct (**4a**) through (**Scheme 2**) reaction of the crude chalcone (**3a**) obtained in step 1 containing 10 mol% of the initially added [DILPOM]-3 catalyst was treated with 1 mmol of indole in neat conditions at two different temperatures i.e. 80 °C and 100 °C (**Table 4.1**, entries 6, 12). It was seen that above 80 °C, the selectivity of product formation was reduced. Step-II of reaction was also studied in water as reaction medium under reflux temperature after step-I was also performed at same reflux conditions. The result showed lower yield of product **4a** (45%) for 8 hours reaction in step-II however with selectively one desired product (**Table 4.1**, entry 13).

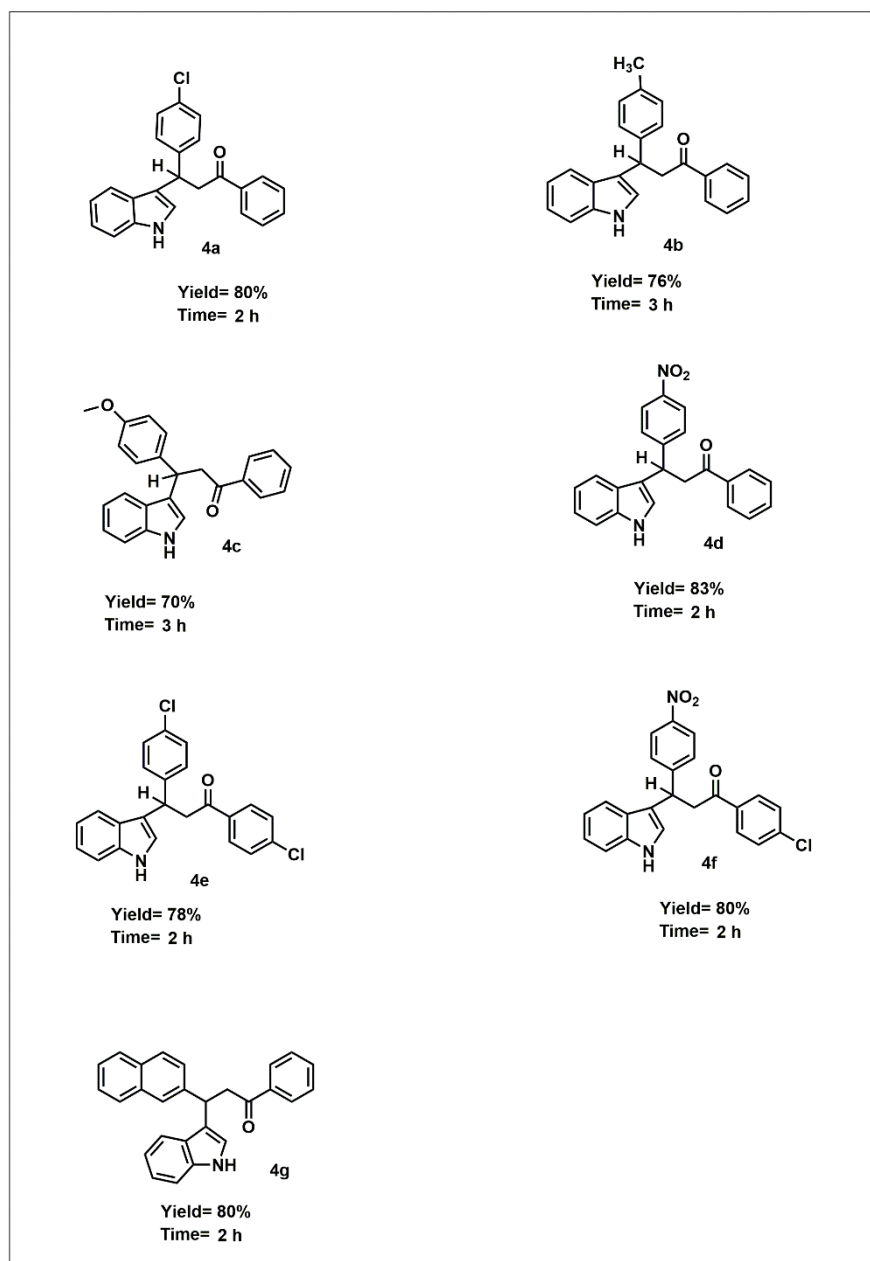
A reaction with 10 mol% of $\text{H}_3\text{PMo}_{12}\text{O}_{40}\cdot 25\text{H}_2\text{O}$ was performed (**Table 4.1**, entry 14) and it was observed that in 1 hour, only 52% of chalcone was produced under solvent-free condition at 80 °C whereas, the other three IL-POM hybrids showed 80-96% yields of the chalcone (**3a**) in 1st step of reaction (**Table 4.1**, entries 2,4,6) using the same amount of catalyst. Therefore, the continuation of 2nd step was not done. From this observation, it can be said that the existence of sulfonic acid groups in the dicationic IL-POM increase their overall acidic sites as compared to the $\text{H}_3\text{PMo}_{12}\text{O}_{40}\cdot 25\text{H}_2\text{O}$. Therefore, the continuation of 2nd step was not done. From this observation, it can be said that the existence of sulfonic acid groups in the dicationic IL-POM increase their overall acidic sites as compared to the $\text{H}_3\text{PMo}_{12}\text{O}_{40}\cdot 25\text{H}_2\text{O}$. However, the reaction with dicationic ionic liquid [DIL-3] was not conducted because when the reaction was tried to be carried out at 80 °C, the reaction emits excessive fumes under solvent free condition. This could possibly because of bound water present in [DIL-3] which produces excess fumes due to HCl gas generation after reaction with labile chloride of the ionic liquid at 80 °C.

This is the reason behind incorporation of sulphonic acid based dicationic ionic liquids into 12-phosphomolybdic acid and generation of IL-POM hybrids, which could be operated at high reaction temperature without emission of any toxic fumes. To avoid hazardous emission of fumes from liquid acids like mineral acids, volatile acidic ionic

liquids, solidification was done by charge balancing the H^+ of 12-molybdophosphoric acid with methylene bridged $-SO_3H$ functionalized imidazolium dication. By doing so, it was aimed to incorporate acidic sites in counter cation which was aimed to minimize byproduct formation. The introduction of various lengths of methylene bridged connecting spacer resulted in tuning the acidity of the $-SO_3H$ acidic sites thus lowering the generation of byproduct. BET study for surface property was done for the active catalyst [DILPOM]-3 as it showed highest percentage yield of (**4a**) in lowest time. It was observed that [DILPOM]-3 has a surface area of $8.264 \text{ m}^2/\text{g}$ which is very low. However, the reactivity of [DILPOM]-3 is attractive and better than pure 12-molybdophosphoric acid. The activity in the hybrids might be a result of modification in the chemical and morphological properties of $[PMo_{12}O_{40}]_3^-$ by incorporation of $-SO_3H$ functionalized methylene chain connecting imidazolium dication. From the FT-IR spectra of the three hybrids (**Fig. 4.1**), it was confirmed that intramolecular hydrogen bond interactions capacity of $-OH$ peak in $-SO_3H$ group of [DILPOM]-3 decreased which resulted in more numbers of free $-SO_3H$ acidic groups and thus the same can be stated as a reason for comparatively higher yields of **3a** followed by **4a** using [DILPOM]-3.

4.3.3 Substrate scope study for sequential Claisen-Schmidt condensation and Michael-like reactions

Substrate scope study for the sequential Claisen-Schmidt condensation and Michael-like reaction was investigated by extending the standard condition of model reaction (**Scheme 4.2**) with substituted aromatic aldehydes as well as acetophenone derivatives in neat conditions at $80 \text{ }^\circ\text{C}$ using 10 mol% of the efficient catalyst [DILPOM]-3. In all cases the formation of chalcones in the 1st step were confirmed by comparison with the authentic samples of chalcones and characterization of intermediates chalcones via spectroscopic techniques. Then addition of the indole to the crude mixture of chalcones produced 80-85% yields of the products within 2-3 hours reaction period (**Fig. 4.13**).



[a] Yield % = Calculated from isolated yield and Time taken in step-II

Fig. 4.13: Substrate scope study of 3-substituted indoles

A comparison table (**Table 4.2**) is provided for comparison of the active catalyst [DILPOM]-3, to some of the reported catalyst in the recent years. Not many reports on two- step, 1-pot synthesis of 3 substituted indole using acetophenone and *p*-chlorobenzaldehyde as initial substrate were found except the one done by our group using -SO₃H functionalized ionic liquid catalyst [27]. Synthesis of 3 substituted indole was obtained without isolation of intermediate chalcone that was reacted with indole. All the examples of the reported catalyst given in the table were used for synthesis of (**4a**) in

which chalcone and indole were the initial substrates. It can be observed that using all the other catalysts, the percentage yield is more compared to the one found in this report. However, the solvent free condition with 3h of reaction time giving 80% of **4a** including *in-situ* generation of chalcone via Claisen-Schmidt condensation followed by Michael-Like addition is a fair one since it is a one-pot two step synthesis protocol for 3-substituted indole.

Table 4.2: Comparison table of the catalyst [DILPOM]-3 with various reported catalysts for synthesis of **4a** using chalcone and indole.

Entry	Catalyst/Temperature/solvent/time/Yield%	Reference
1.	Arene Diazonium Tetrafluoroborate Salts/60 °C/MeOH/24 h/86%	68
2.	Fe(OTf) ₃ ·6H ₂ O/100 °C/Eucalyptol/45 min/90%	69
3.	Al ₂ O ₃ / 68 °C/Hexane/6 h/91%	70
4.	KHSO ₄ /r.t./C ₂ H ₅ OH/6.5h/85%	71
5.	Polyvinylsulfonic acid/reflux/ C ₂ H ₅ OH/6h/92%	21
6.	[DILPOM]-3/80 °C/solvent-free/3h/80%	^a Current work

^aReaction time indicates synthesis of **4a** including Claisen-Schmidt reaction (*in-situ* generation of chalcone) followed by Michael-like addition.

4.4 Recyclability study of the catalyst

The recyclability experiment of [DILPOM]-3 catalyst was done by taking equal number of substrate (1 mmol) of the model reaction (**Scheme 4.2**) to conduct Claisen-Schmidt condensation to prepare the chalcone derivative for Michael-Like addition with 1 mmol of indole under the optimized conditions in solvent-free method. The used catalyst being insoluble in all organic solvents can be separated easily from the solution of reaction mixture in ethyl acetate by simple centrifugation. The catalyst was recycled for four catalytic cycle with 1 hour in step-I and 2 hours in step-II and the % yields of **4a** at the end of step-II was calculated and provided in (**Fig. 4.14**). The FT-IR spectrum of the spent catalyst after the 4th cycle showed high intensity peak at 3458 cm⁻¹ compared to fresh catalyst that infers incorporation of H₂O molecules inside the organic-inorganic hybrid (**Fig. 4.15**).

From the ³¹P NMR of fresh catalyst [DILPOM]-3, one high intensity peak was observed at -4.11 ppm for [PMo₁₂O₄₀]³⁻ anion along with one small peak at -0.35 ppm. Whereas in the spent catalyst after 4th catalytic cycle, the up-field peak shifted its position from -4.11 to -3.53 ppm (**Fig. 4.16**). This deshielding is a result of presence of hydration sphere in and around the hybrid after subsequent catalytic cycles. Along with that two more peaks were observed in the spectrum at -2.01 ppm for [P₂Mo₁₈O₆₂]⁶⁻ and -0.77 ppm for

$[\text{PMo}_{11}\text{O}_{39}]^{7-}$ [72]. With subsequent use of [DILPOM]-3 over time, some of the $[\text{PMo}_{12}\text{O}_{40}]^{3-}$ unit with Keggin structure changed considerably to Wells-Dawson anion structure $[\text{P}_2\text{Mo}_{18}\text{O}_{62}]^{6-}$ [72]. The peak at -0.45 ppm in $\text{H}_3\text{PMo}_{12}\text{O}_{40}$ is tentatively an impurity that has been detected for presence of $[\text{PMo}_{11}\text{O}_{39}]^{7-}$ when synthesis of $\text{H}_3\text{PMo}_{12}\text{O}_{40}$ was done under strongly acidic condition [73]. And the same impurity peak existed in spent [DILPOM]-3 and shifted to -0.77 ppm in the spent catalyst. With subsequent use of [DILPOM]-3 over time, decomposition of $[\text{PMo}_{12}\text{O}_{40}]^{3-}$ unit with Keggin structure considerably to $[\text{P}_2\text{Mo}_{18}\text{O}_{62}]^{6-}$ and $[\text{PMo}_{11}\text{O}_{39}]^{7-}$ occurred.

Discussing about the NH_3 -TPD results of the spent catalyst (**Fig. 4.17**), they showed the existence of acidic sites similar to NH_3 -TPD graph of the unused [DILPOM]-3 presented under section **4.2.10 Determination of acidic sites of hybrids**, even after consecutive cycles of recyclability reactions. Therefore, no deactivation of catalytic active sites has been noted for the spent catalyst, however a new peak at 325 °C was observed which might be because of the acidic sites after conversion of spent [DILPOM]-3 into other forms as observed from ^{31}P NMR of spent catalyst. The decrease in yield over the cycles might be a result of other factors like surface contamination, decrease in substrate-catalyst interaction due to association of physisorbed water thus increasing hydrophilicity in the catalyst.

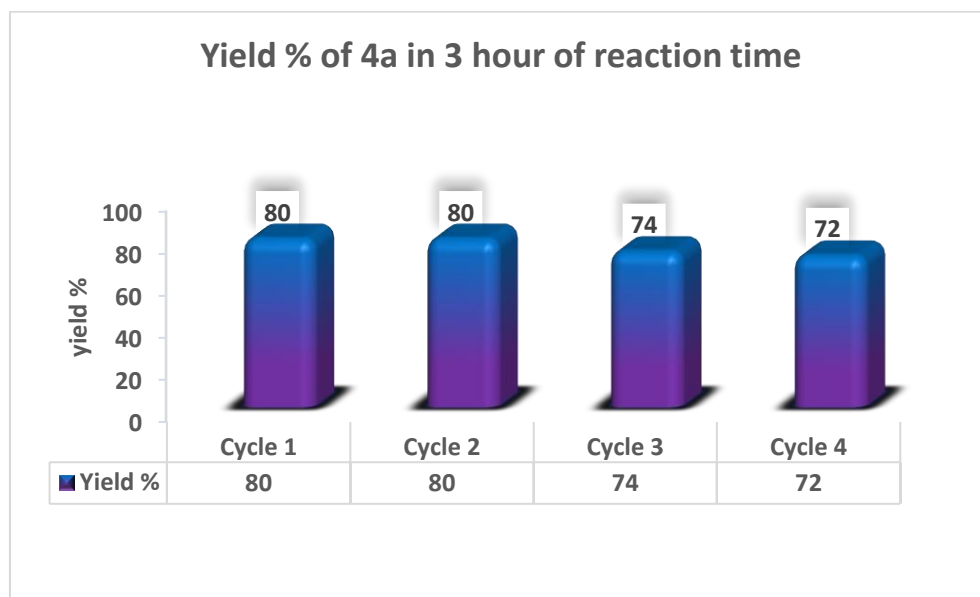


Fig. 4.14: Bar diagram for recyclability of catalyst.

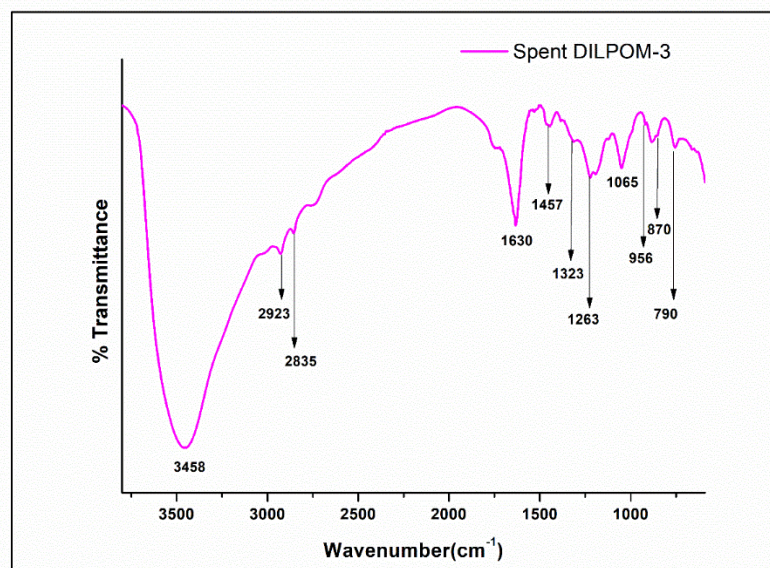


Fig. 4.15: FT-IR spectrum of recycled [DILPOM]-3 after 4th catalytic cycle.

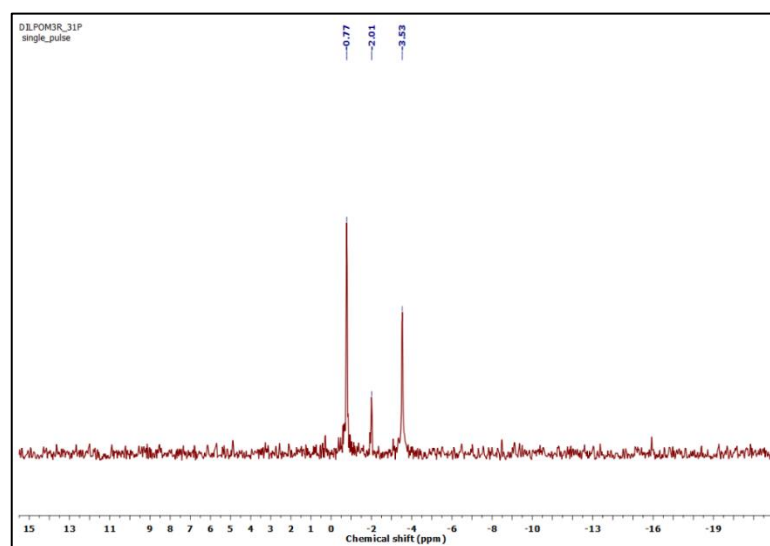


Fig. 4.16: ³¹P NMR of the spent [DILPOM]-3 after 4th catalytic cycle.

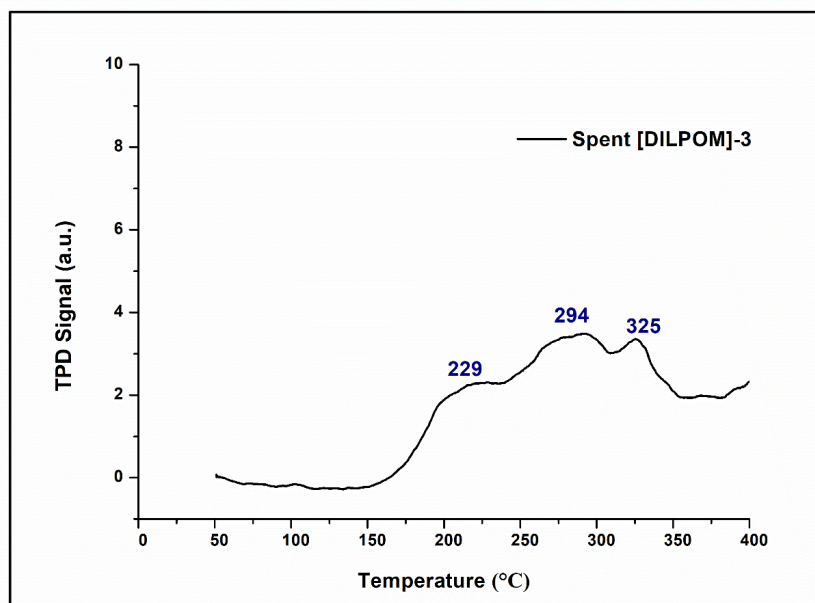
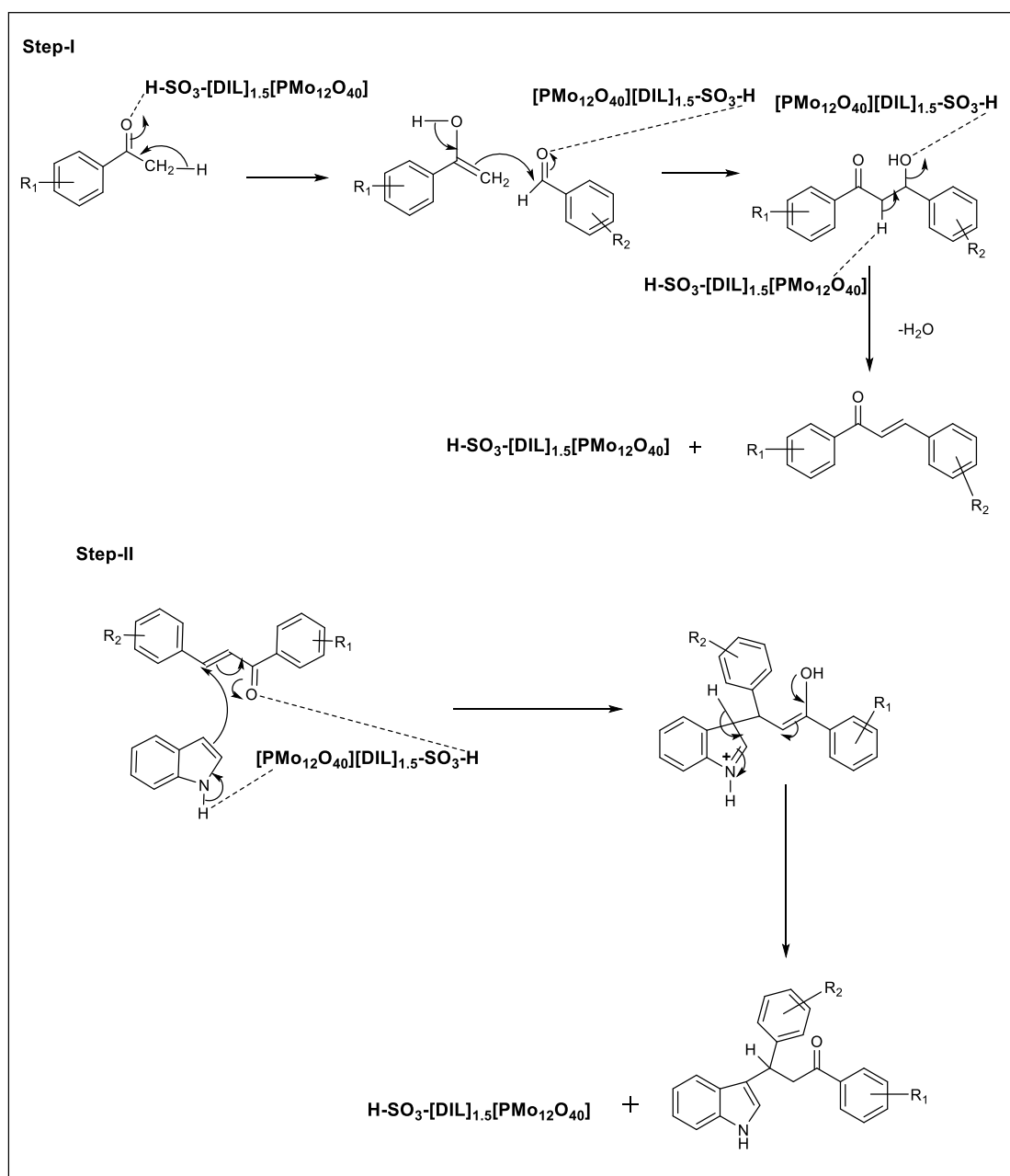


Fig. 4.17: NH₃-TPD of the spent [DILPOM]-3 catalyst after 4th catalytic cycle.

4.5 Plausible reaction mechanism

The plausible mechanism of sequential two step reactions of the Claisen-Schmidt condensation can be described in **Scheme 4.3** through conversion of acetophenone to its enol form by interactions with the Brønsted-Lewis acidic sites of the IL-POM catalysts and then synergic effects of the same acidic sites of catalyst for activation of nucleophilic attack to carbonyl group of aromatic aldehydes with the enol form of acetophenone molecule. This is followed by the acidic site-initiated dehydration of β -hydroxy keto compounds to chalcone derivatives. The next step Michael-like addition of indole can be assumed from activation of the carbonyl group of chalcones involving hydrogen bond interactions with the -SO₃H group of catalyst as well as also interconnection of N-H proton of the indole with the PMO₁₂O₄₀³⁻ anion (**Scheme 4.3**) that lead to formation of Michael adduct.



Scheme 4.3: Plausible mechanism of sequential one-pot synthesis of Michael-adduct via Claisen-Schmidt Condensation.

4.6 Conclusions

In this work, three organic-inorganic hybrid materials of POM-ILs were synthesized with variable lengths of the methylene bridged imidazolium dications and $[\text{PMo}_{12}\text{O}_{40}]^{3-}$ anion. The composition of hybrid material was confirmed from its ^1H , ^{13}C NMR spectra as well as CHN analysis. The catalytic activity of these acidic heterogenous hybrids were explored in the sequential Claisen-Schmidt condensation followed by Michael-Like addition of indole with chalcone to prepare 3-substituted indoles as single product in one pot method

without isolation of the intermediate chalcones using 10 mol % of the catalyst at 80 °C within 3-4 hours for different substrates in neat conditions. The catalyst was recycled for three runs and decrease of catalytic activity was observed over the cycles. No oxidative products were isolated during reaction which clearly displayed preferential role of Brønsted acidity of the hybrid for the acid catalysed reaction. The acidic nature of the POM-IL hybrid can be explored to conduct variety of Brønsted acid catalysed organic reactions including multicomponent synthesis of heterocycles, protection-deprotection chemistry, functional group conversion etc. Similarly, there is a scope to examine the redox properties of this catalyst for oxidation of alcohol, alkene etc. in presence of environmentally benign oxidant.

The cationic composition in the organic part of the hybrid and the interactions of $\text{-SO}_3\text{H}$ functional groups present with the anionic $\text{PMo}_{12}\text{O}_{40}^{3-}$ results in the overall acidity, solubility in solvent. Since the cationic part comprises of the $\text{-SO}_3\text{H}$ group, so the cationic part is responsible for the general acidity in the hybrid. The hybrid with the longer alkyl bridged spacer [DILPOM]-3 showed the highest catalytic activity which is the result of acidity evidenced by FT-IR studies using pyridine as probe molecule and NH_3 -TPD graphs. These results infer that due to presence of longer carbon chain in [DILPOM]-3, steric hindrance increases which weakens the interactions between the counterions, resulting in a greater number of free $\text{-SO}_3\text{H}$ groups which in turn resulted in highest yield of 4a. The high thermal stability of [DILPOM]-3 gives the prospect for carrying out other acid catalysed organic reactions in near future. However, the structural decomposition of catalyst over a few catalytic cycles, serves as a disadvantage for these catalysts.

4.7 Experimental section

4.7.1 Procedure for synthesis of [DILPOM]-1, [DILPOM]-2, [DILPOM]-3 where POM is Keggin $[\text{PMo}_{12}\text{O}_{40}]^{3-}$ anion

At the beginning, an equimolar mixture of 2-methylimidazole (2 mmol) and 2 mmol of NaH was stirred in dry THF (95%) (10 mL) as solvent at room temperature for 30 minutes (**Scheme 4.1**). The solvent was then evaporated under reduced pressure and the residue obtained was washed with diethyl ether for two to three times and thus purest form of sodium salt of 2- methylimidazole (A) was obtained after drying in vacuum oven. Afterwards, three separate batches of pure sodium salt of 2-methylimidazole were prepared. Three separate batch of obtained sodium salt of 2-methylimidazole was treated

with (1 mmol) of dibromopropane / dibromobutane /dibromododecane respectively to observe the effect of long vs short chain length of methylene bridging group using THF (20 mL) as solvent. The mixture was refluxed for 10 hours and then filtered. The filtrate was washed with diethyl ether for three times and then evaporated under reduced pressure to get the respective intermediates B/ C/ D as brown solid. In the next step, ClSO_3H (2 equivalent) was added dropwise to 1 equivalent of intermediate B/C/D respectively in dry DCM (20 mL) used as reaction solvent. The reaction mixture was stirred for 8 hours in room temperature. After 8 hours, a separate layer of the respective ionic liquids generated, insoluble in DCM layer was observed and unreacted chlorosulphonic acid with alkyl-bridged diimidazole remains soluble in the DCM layer. The solvent was removed under vacuum and the reaction mixture was washed three times (3×5 mL) with dry DCM to remove the DCM soluble impurities. Thus, the parent dicationic chloride ionic liquids (DIL-1/DIL-2/DIL-3) i.e., E/F/G respectively were obtained. The last step is the metathesis step in which an aqueous solution (10 mL) of 1 equivalent of $\text{H}_3\text{PMo}_{12}\text{O}_{40} \cdot n\text{H}_2\text{O}$ is added to 1.5 equivalent of E/F/G or $[\text{DIL-1}] \cdot n\text{H}_2\text{O}$ / $[\text{DIL-2}] \cdot n\text{H}_2\text{O}$ / $[\text{DIL-3}] \cdot n\text{H}_2\text{O}$ at room temperature. Immediate precipitation is observed in each case. The reactions were allowed to stir for next 12 hours at room temperature. After that, the water insoluble crude products were centrifuged, washed, and dried in vacuum oven to get the solid material $[\text{DILPOM}]-1/2/3$ in their purest form. The samples were analysed by FT-IR, ^1H NMR, ^{13}C NMR and various other analytical techniques.

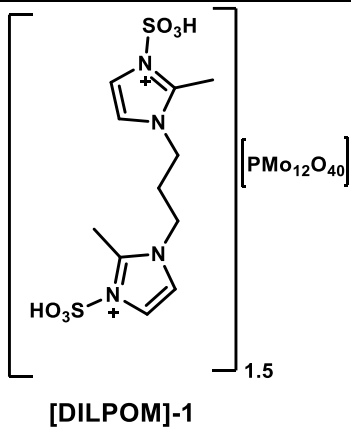
4.7.2 Typical procedure for synthesis of 3-substituted indoles

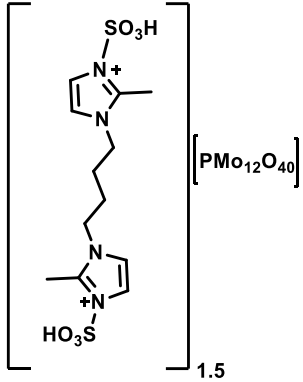
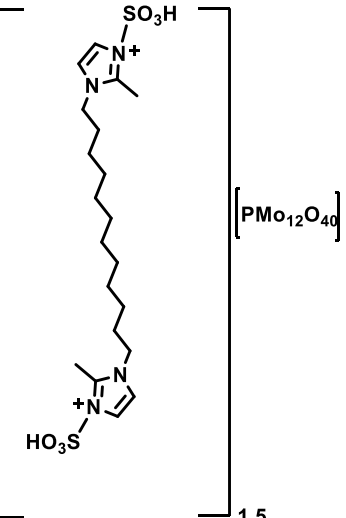
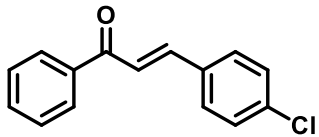
A mixture of 4-Cl benzaldehyde (1 mmol) and acetophenone (1 mmol) was reacted in a 50 mL two necked round bottom flask in solvent-free condition at 80°C in presence of 10 mol% of $[\text{DILPOM}]-3$ for selective formation of intermediate chalcones in 1h, as confirmed from Thin Layer Chromatography (TLC) technique through comparison with the authentic chalcone. The crude chalcone mixture obtained in the 1st step was followed by addition of 1 mmol of indole to undergo Michael-like addition reaction to get the required product i.e., 3-substituted indole within next 2h. After completion of the reaction as monitored from TLC, the reaction mixture was diluted with EtOAc (5 mL) to dissolve the organic product only. The isolation of catalyst was done by centrifugation, as the catalyst remains insoluble in EtOAc. The catalyst was recovered by simple decantation of the EtOAc solution and washed the used catalyst with additional EtOAc (2×3 mL) water as well as DCM in turns to remove impurities and then dried in vacuum oven before using

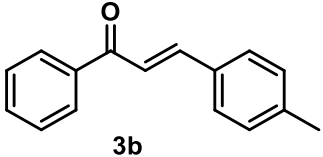
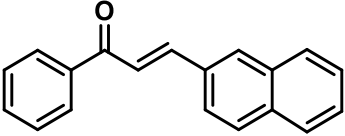
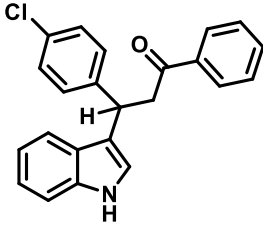
it for next runs. The EtOAc extract of product mixture was washed with water (10 mL) and dried over anhydrous sodium sulfate to remove any traces of water. The evaporation of EtOAc extract under reduced pressure gave the crude product mixture which was further purified by column chromatography to get analytically pure product with 80% yield.

4.8 Spectral Data

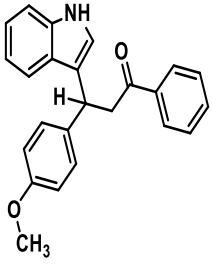
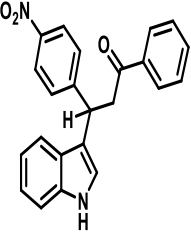
Table 4.3: Spectral data of IL-POM hybrids, selected chalcones, Michael adducts

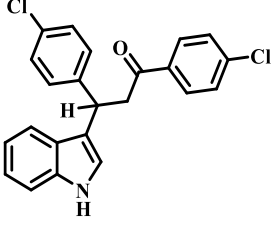
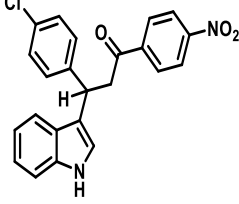
Spectral data of [DILPOM]-1, [DILPOM]-2 and [DILPOM]-3	
Products	Spectral data
 <p>[DILPOM]-1</p>	<p>Yellow colored solid; melting point >300 °C</p> <p>¹H NMR (400 MHz, DMSO-<i>d</i>₆) δ (ppm): 13.91(s, 2H), 7.58-7.48 (m, 4H), 4.13 (t, <i>J</i> = 8Hz, 4H), 2.56 (s, 6H), 2.46 (s, 2H).</p> <p>¹³C NMR (100 MHz, DMSO-<i>d</i>₆) δ (ppm): 144.8, 122.1, 118.7, 44.5, 29.3, 10.8.</p> <p>³¹P NMR (202 MHz DMSO-<i>d</i>₆) δ (ppm): - 4.12.</p> <p>[DILPOM]-1, calculated: C 8.37%, H 1.14%, N 3.55%, found: C 8.23% H 1.24% N 3.12%.</p>

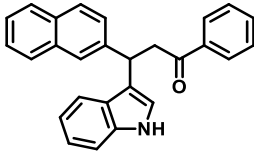
 <p>[DILPOM]-2</p>	<p>Yellow colored solid; melting point > 300 °C</p> <p>¹H NMR (400 MHz, DMSO-<i>d</i>₆) δ (ppm): 13.85 (s, 2H), 7.61-7.45 (m, 4H), 4.10 (s, 4H), 2.46 (s, 6H), 1.75 (s, 4H).</p> <p>¹³C NMR (100 MHz, DMSO-<i>d</i>₆) δ (ppm): 119.2, 100.0, 11.7.</p> <p>³¹P NMR (202 MHz, DMSO-<i>d</i>₆) δ (ppm): -4.11.</p> <p>[DILPOM]-2, calculated: C 9.05%, H 1.25%, N 3.52%, found: C 9.28% H 1.45% N 3.75%.</p>
 <p>[DILPOM]-3</p>	<p>Yellow colored solid; melting point > 300 °C</p> <p>¹H NMR (400 MHz, DMSO-<i>d</i>₆) δ (ppm): 13.84 (s, 2H), 7.59-7.45 (m, 4H), 4.01 (s, 4H), 2.43 (s, 6H), 1.66 (s, 4H), 1.18 (s, 16H).</p> <p>¹³C NMR (100 MHz, DMSO-<i>d</i>₆) δ (ppm): 144.3, 122.4, 118.6, 119.2, 29.4, 10.8.</p> <p>³¹P NMR (202 MHz, DMSO-<i>d</i>₆) δ (ppm): -4.11.</p> <p>[DILPOM]-3, calculated: C 10.19%, H 2.12%, N 3.18%, found: C 11.12% H 2.98% N 3.19%.</p>
Spectral data of selected chalcones	
 <p>(E)-3-(4-chlorophenyl)-1-phenylprop-2-en-1-one</p> <p>3a</p>	<p>Yellow colored solid; M.p. 113 °C</p> <p>¹H NMR (400 MHz, CDCl₃) δ (ppm): 8.00 (d, <i>J</i> = 8Hz, 2H); 7.74 (d, <i>J</i> = 16Hz, 1H), 7.58-7.47(m, 6H), 7.38 (d, <i>J</i> = 8Hz, 2H).</p>

	¹³ C NMR (100 MHz, CDCl ₃) δ (ppm): 190.3, 143.4, 138.1, 133.4, 133.0, 129.7, 129.3, 128.8, 128.6, 122.5.
 <p>3b (E)-1-phenyl-3-(p-tolyl)prop-2-en-1-one</p>	<p>Yellow colored solid; M.p. 90 °C</p> <p>¹H NMR (400 MHz, CDCl₃) δ (ppm): 8.01(d, <i>J</i> = 8Hz, 2H), 7.79 (d, <i>J</i> = 16 Hz, 1H), 7.57-7.46 (m, 5H), 7.22 (d, <i>J</i> = 8Hz, 3H), 2.39 (s, 3H).</p> <p>¹³C NMR (100 MHz, CDCl₃) δ (ppm): 190.8, 145.0, 141.2, 138.3, 131.9, 128.8, 21.7.</p>
 <p>3g (E)-3-(naphthalen-2-yl)-1-phenylprop-2-en-1-one</p>	<p>Yellow colored solid; M.p. 153 °C</p> <p>¹H NMR (400 MHz, CDCl₃) δ (ppm): 8.07-8.04 (m, 3H), 7.98 (d, <i>J</i> = 16Hz, 1H), 7.88-7.81(m, 4H), 7.65 (d, <i>J</i> = 16 Hz, 1H), 7.59 (d, <i>J</i> = 8Hz, 1H), 7.54-7.51(m, 4H).</p> <p>¹³C NMR (100 MHz, CDCl₃) δ (ppm): 190.6, 145.1, 138.4, 134.5, 132.9, 130.83, 129.2, 128.8, 128.6, 127.9, 127.5, 126.9, 123.7, 122.3.</p>
Spectral data of Michael adduct (4a-4g)	
 <p>4a 3-(4-chlorophenyl)-3-(1H-indol-3-yl)-1-phenylpropan-1-one</p>	<p>Light pink colored solid; M.p. 129 °C</p> <p>¹H NMR (400 MHz, CDCl₃) δ (ppm): 8.02 (s, 1H), 7.94 (d, <i>J</i> = 8Hz, 2H), 7.57 (t, <i>J</i> = 8Hz, 1H), 7.47-7.40 (m, 3H); 7.35 (d, <i>J</i> = 8Hz, 1H), 7.30 (d, <i>J</i> = 8Hz, 2H), 7.21 (d, <i>J</i> = 8Hz, 2H), 7.18 (t, <i>J</i> = 8Hz, 1H),</p>

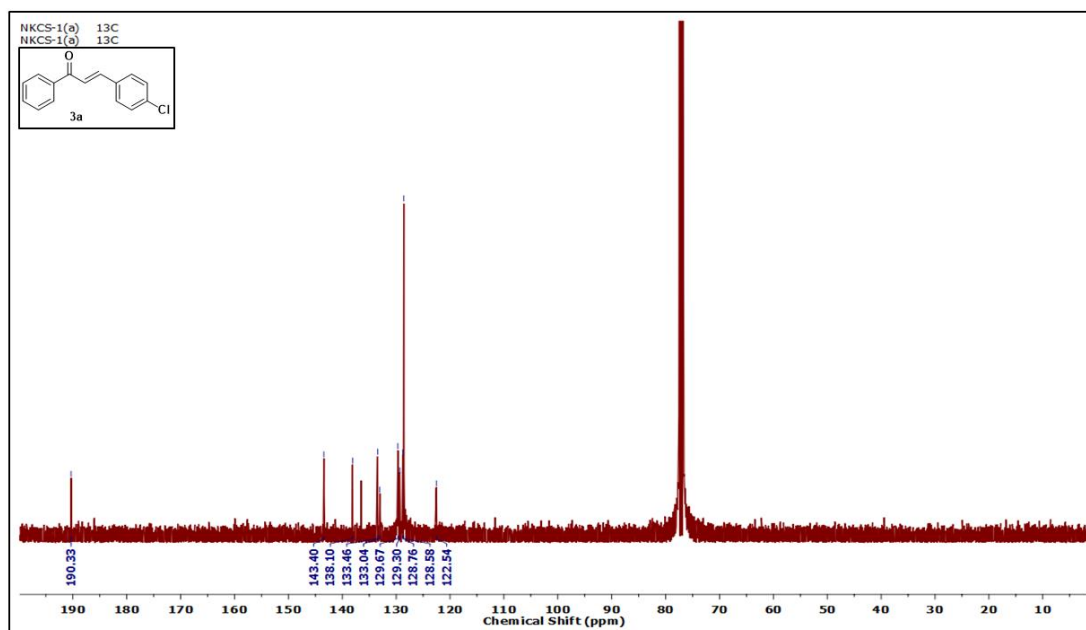
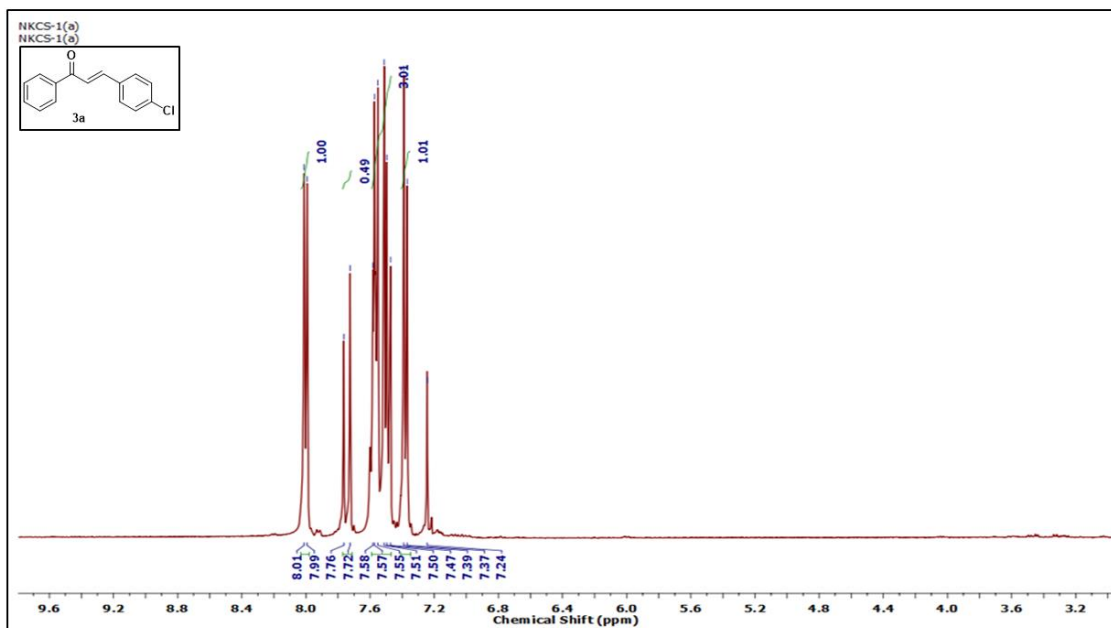
	<p>7.06-7.04 (m, 2H), 5.08-5.04 (m, 1H), 3.85-3.79 (dd, $J = 16\text{Hz}$, 8Hz, 1H), 3.74-3.68 (dd, $J = 16\text{Hz}$, 8Hz, 1H).</p> <p>^{13}C NMR (100 MHz, CDCl_3) δ (ppm): 198.5, 142.7, 136.8, 131.9, 131.8, 130.2, 128.5, 128.2, 127.0, 126.5, 123.7, 122.2, 12.0, 119.2, 119.0, 111.2, 39.7, 21.2.</p> <p>CHN analysis: Calculated for 4a, $\text{C}_{23}\text{H}_{18}\text{NOCl}$: C 76.77, H 5.04, N 3.89; Found: C 76.1, H 5.31, N 3.60.</p>
<p>3-(1H-indol-3-yl)-1-phenyl-3-(p-tolyl)propan-1-one</p> <p>4b</p>	<p>Dark pink colored solid; M.p. 133 °C</p> <p>^1H NMR (400 MHz, CDCl_3) δ (ppm): 7.96 (s, 1H), 7.90 (d, $J = 8\text{Hz}$, 2H), 7.49 (t, $J = 8\text{Hz}$, 1H), 7.44-7.36 (m, 3H), 7.20 (t, $J = 8\text{Hz}$, 3H), 7.10 (t, $J = 8\text{Hz}$, 1H), 7.04-6.96 (m, 3H), 6.86 (s, 1H), 5.03-4.99 (m, 1H), 3.79-3.74 (dd, $J = 16\text{Hz}$, 8Hz, 1H), 3.70-3.64 (dd, $J = 16\text{Hz}$, 8Hz, 1H), 2.24 (s, 3H).</p> <p>^{13}C NMR (100 MHz, CDCl_3) δ (ppm): 199.3, 141.3, 137.2, 136.8, 135.9, 135.6, 128.7, 128.3, 127.2, 126.7, 123.8, 121.9, 120.0, 119.8, 119.2, 111.3, 60.7, 39.9, 21.2.</p> <p>CHN analysis: Calculated for 4b, $\text{C}_{24}\text{H}_{21}\text{NO}$: C 84.92, H 6.24, N 4.13; Found: C 84.53, H 6.33, N 4.08.</p>

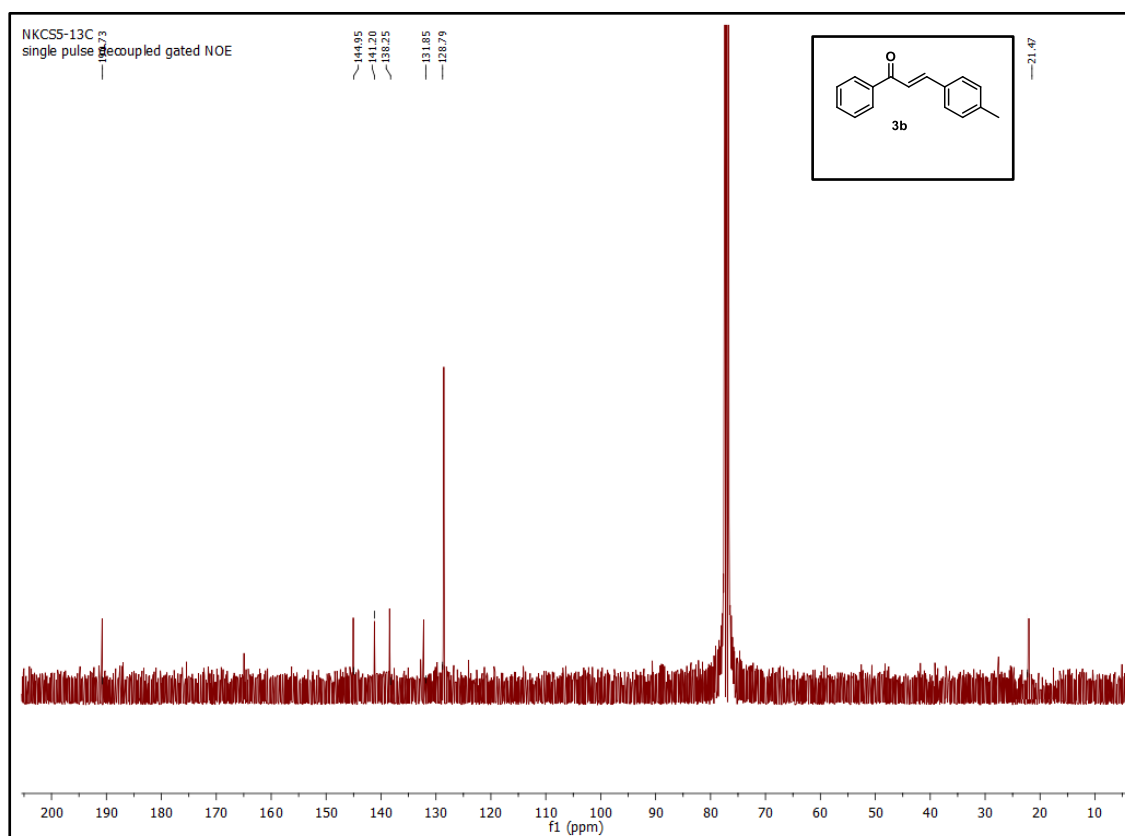
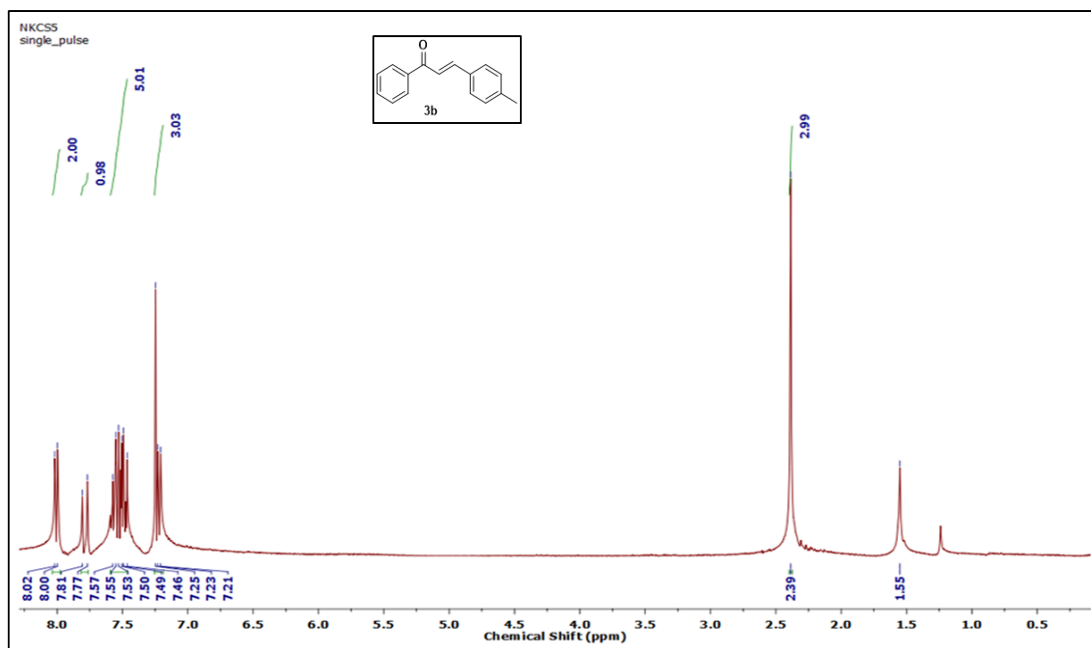
 <p>3-(1H-indol-3-yl)-3-(4-methoxyphenyl)-1-phenylpropan-1-one</p> <p>4c</p>	<p>Dark pink colored solid; M.p. 132 °C</p> <p>¹H NMR (400 MHz, CDCl₃) δ (ppm): 7.89 (s, 1H), 7.38 (d, <i>J</i> = 8Hz, 2H), 7.33 (d, <i>J</i> = 8Hz, 2H), 7.25-7.23 (m, 2H), 7.16 (t, <i>J</i> = 8Hz, 2H), 6.99 (t, <i>J</i> = 8Hz, 2H), 6.81(d, <i>J</i> = 8 Hz, 2H), 6.62 (s, 2H), 5.83 (s,1H), 4.15-4.09 (m, 2H), 3.77 (s, 3H).</p> <p>¹³C NMR (100 MHz, CDCl₃) δ (ppm): 171.6, 158.2, 137.1, 136.4, 135.2, 129.9, 126.5, 123.6, 121.7, 120.2, 119.1, 113.4, 111.2, 110.8, 54.9, 39.5.</p> <p>CHN analysis: Calculated for 4c, C₂₄H₂₁NO₂: C 81.10, H 5.96, N 3.94; Found: C 81.26, H 5.75, N 3.60.</p>
 <p>3-(1H-indol-3-yl)-3-(4-nitrophenyl)-1-phenylpropan-1-one</p> <p>4d</p>	<p>Light yellow colored solid; M.p. 166 °C</p> <p>¹H NMR (400 MHz, CDCl₃) δ (ppm): 8.10 (s, 1H), 7.96 (d, <i>J</i> = 8Hz, 2H), 7.55 (t, <i>J</i> = 8Hz, 1H), 7.37-7.45 (m, 5H), 7.30(d, <i>J</i> = 8Hz, 1H), 7.12-7.16 (m, 2H); 6.97-7.08 (m, 3H), 5.45-5.49 (m, 1H), 3.82-3.76 (dd, <i>J</i> = 16Hz, 8Hz, 1H), 3.65-3.59 (dd, <i>J</i> = 16Hz, 8Hz, 1H)</p> <p>¹³C NMR (100 MHz, CDCl₃) δ (ppm): 197.9, 140.4, 136.8, 136.7, 134.3, 133.3, 132.6, 130.0, 129.6, 128.8, 128.2, 127.3, 126.6, 126.5, 117.3, 111.3, 60.5, 44.0, 34.6.</p>

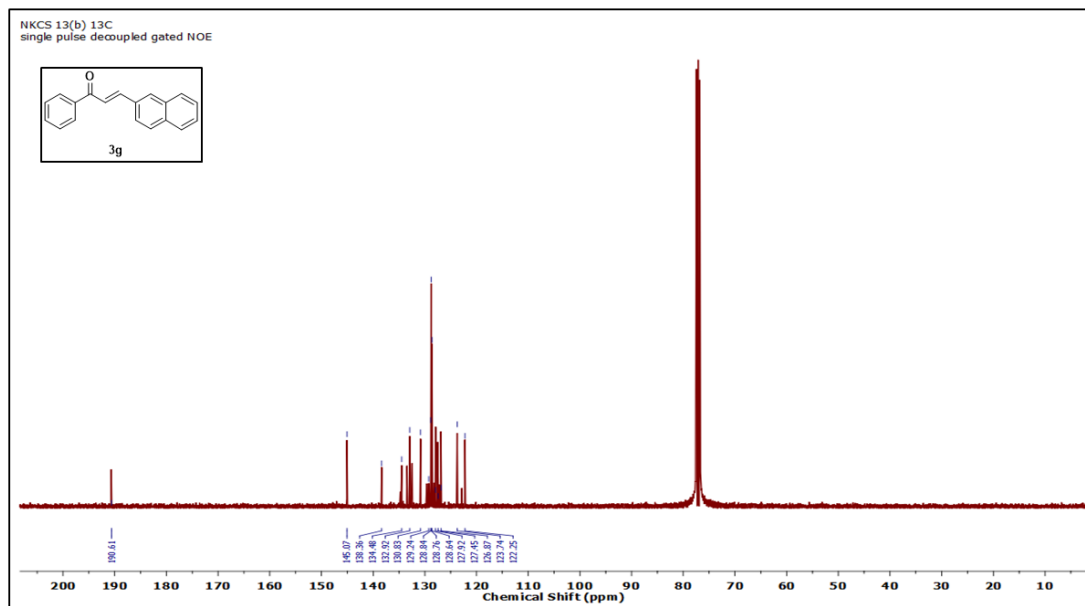
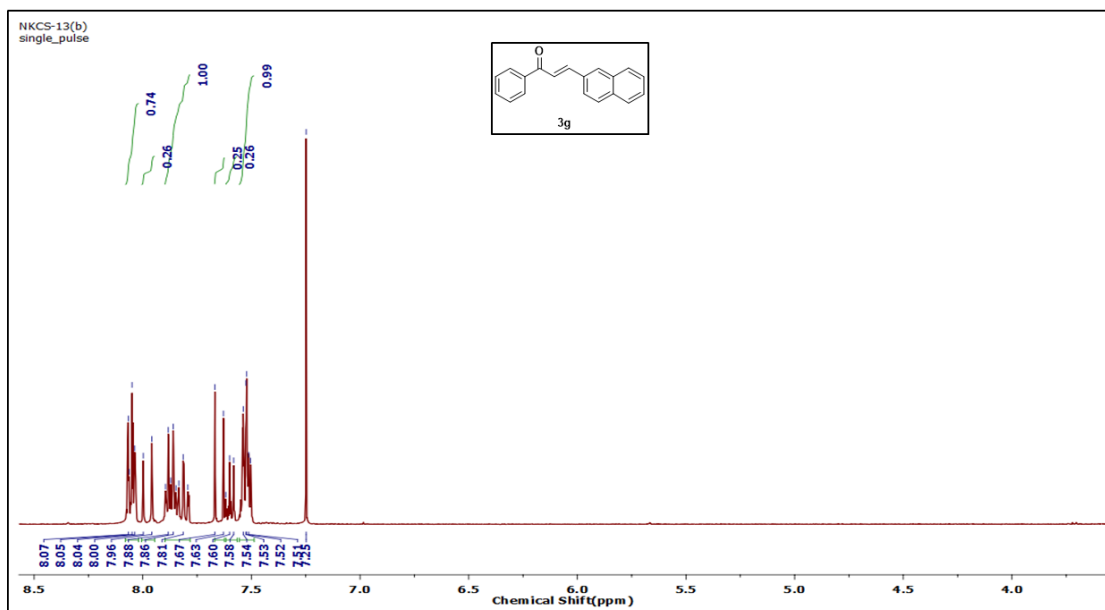
	CHN analysis: Calculated for 4d , $C_{23}H_{18}N_2O_3$: C 74.58, H 4.90, N 7.56 Found: C 74.42, H 4.77, N 7.39
<div style="text-align: center;">  <p>1,3-bis(4-chlorophenyl)-3-(1H-indol-3-yl)propan-1-one</p> <p>4e</p> </div>	Light yellow solid, M.p. 126 °C; 1H NMR (400 MHz, $CDCl_3$) δ (ppm): 8.06 (s, 1H), 7.84 (d, $J = 8$ Hz, 2H), 7.39(d, $J = 8$ Hz, 3H), 7.14-7.31(m, 6H), 7.03 (t, 1H, $J = 8$ Hz), 6.93-6.94 (m, 1H), 5.00-5.04 (m, 1H), 3.79-3.73(dd, $J = 16$ Hz, 8Hz, 1H), 3.68-3.62 (dd, $J = 16$ Hz, 8Hz, 1H). ^{13}C NMR (100 MHz, $CDCl_3$) δ (ppm): 197.4, 142.7, 139.8, 136.7, 135.4, 132.1, 129.6, 129.3, 129.0, 128.7, 126.4, 122.5, 121.5, 119.7, 118.7, 111.4, 100.0, 44.9, 37.7. CHN analysis: Calculated for 4e , $C_{23}H_{18}NOCl_2$: C 70.06, H 4.35, N 3.55; Found: C 70.1, H 4.22, N 3.60.
<div style="text-align: center;">  <p>3-(4-chlorophenyl)-3-(1H-indol-3-yl)-1-(4-nitrophenyl)propan-1-one</p> <p>4f</p> </div>	Light orange solid, M.p. 167 °C; 1H NMR (400 MHz, $CDCl_3$) δ (ppm): 8.01 (s, 1H), 7.96 (d, $J = 8.0$ Hz, 2H), 7.55 (t, $J = 8.0$ Hz, 1H), 7.46-7.37 (m, 4H) 7.13(t, $J = 8.0$ Hz, 1H), 7.09-7.07(m, 2H), 7.06 (s, 1H), 7.02 (t, $J = 8.0$ Hz, 2H), 5.48-5.45 (m, 1H), 3.82-3.76 (dd, $J = 16$ Hz, 8Hz,1H), 3.65-3.59 (dd, $J = 16$ Hz, 8Hz, 1H). ^{13}C NMR (100 MHz, $CDCl_3$) δ (ppm): 196.5, 151.9, 146.4, 140.0, 136.7, 135.1, 130.1, 129.5, 129.1,

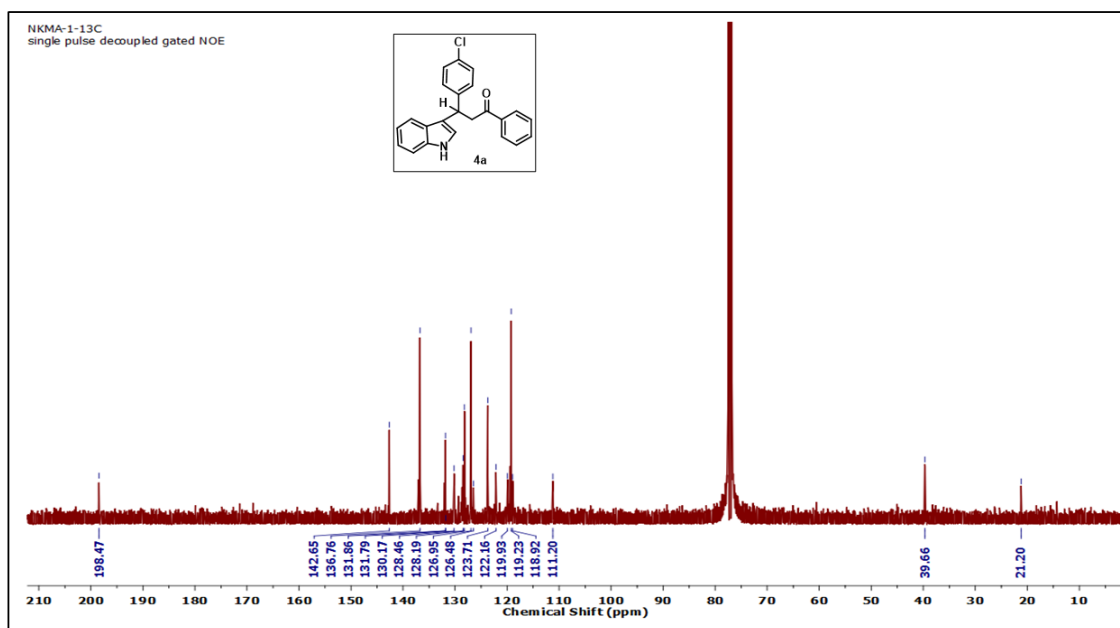
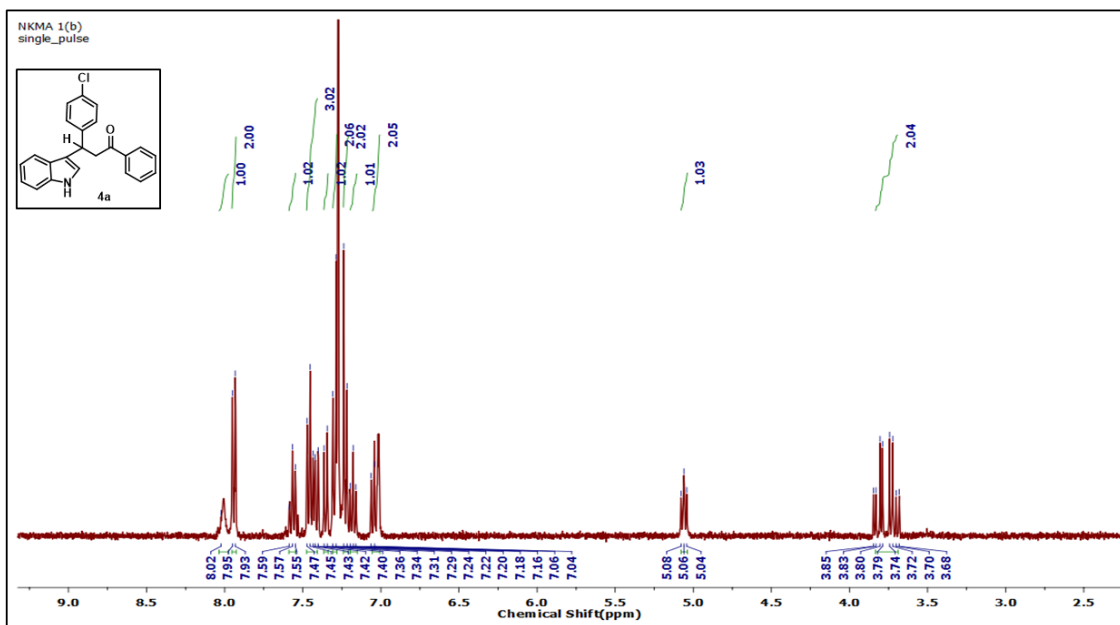
	<p>128.8, 126.2, 123.9, 121.5, 117.9, 44.5.</p> <p>CHN analysis: Calculated for 4f, C₂₃H₁₇N₂O₃Cl: C 68.24, H 4.23, N 6.92; Found: C 68.10, H 4.11, N 6.88.</p>
<p> 3-(1<i>H</i>-indol-3-yl)-3-(naphthalen-2-yl)-1-phenylpropan-1-one 4g</p>	<p>Pink colored solid; M.p. 156.2 °C;</p> <p>¹H NMR (400 MHz, CDCl₃) δ (ppm): 8.0 (s, 1H), 7.94 (d, <i>J</i> = 8 Hz, 1H), 7.79 (s, 1H), 7.76-7.71 (m, 2H), 7.54- 7.38 (m, 7H), 7.32-7.30 (m, 1H), 7.13 (t, <i>J</i> = 8.0 Hz, 1H), 7.01-6.96 (m, 2H) 5.24 (t, <i>J</i> = 8.0 Hz, 1H), 3.93-3.87 (dd, <i>J</i> = 16Hz, 8Hz, 1H), 3.85-3.79 (dd, <i>J</i> = 16Hz, 8Hz, 1H).</p> <p>¹³C NMR (100 MHz, CDCl₃) δ (ppm): 198.59, 170.00, 141.79, 137.21,136.73,133.60,132.38,128.20,126.74, 126.03, 121.70, 121.60, 119.28, 45.14.</p> <p>CHN analysis: Calculated for 4g, C₂₇H₂₁NO: C 86.37, H 5.64, N 3.73; Found: C 86.21, H 5.31, N 3.54.</p>

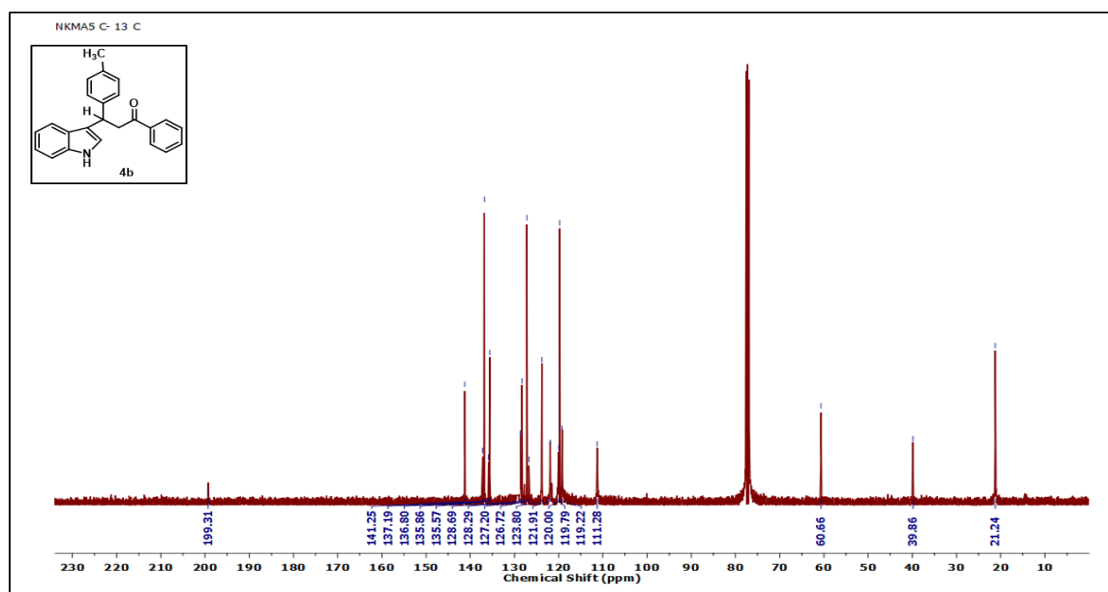
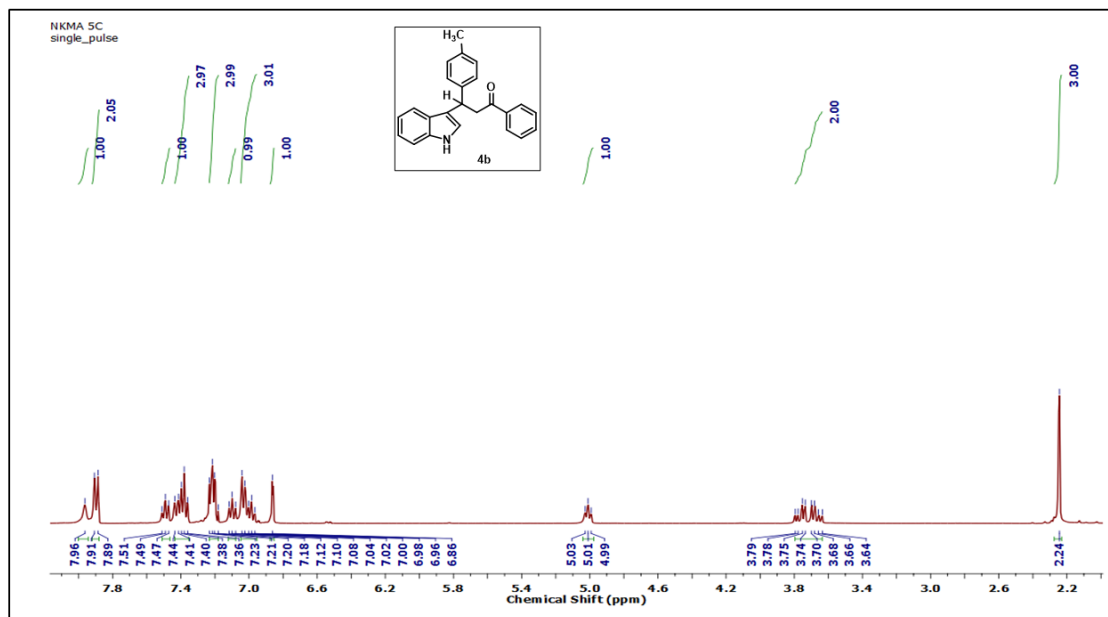
4.9 NMR spectra of selected chalcones and Michael adducts

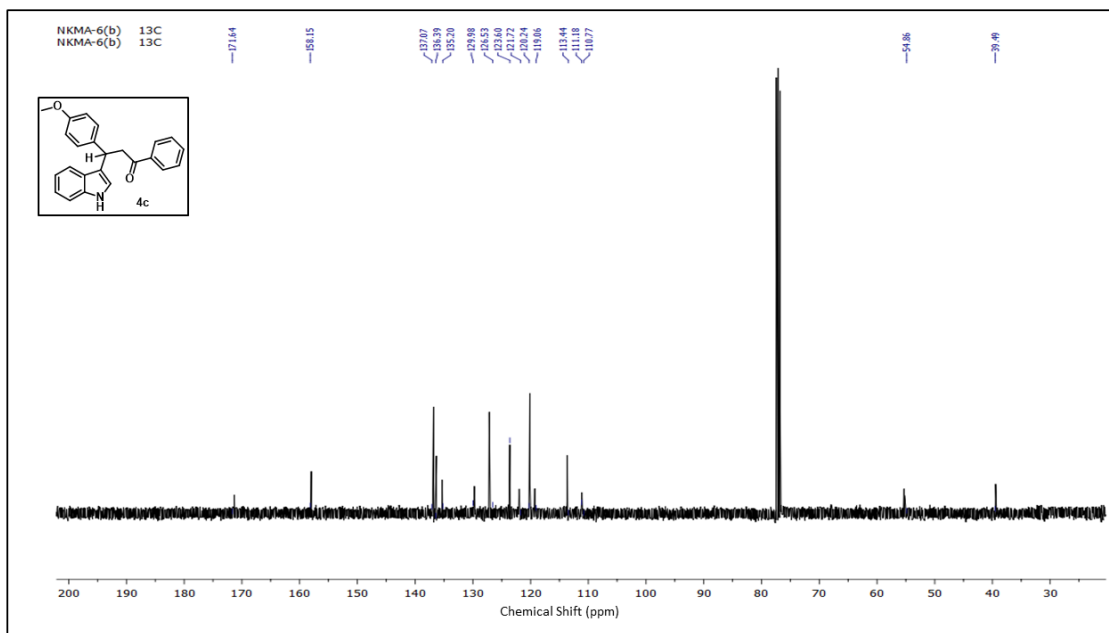
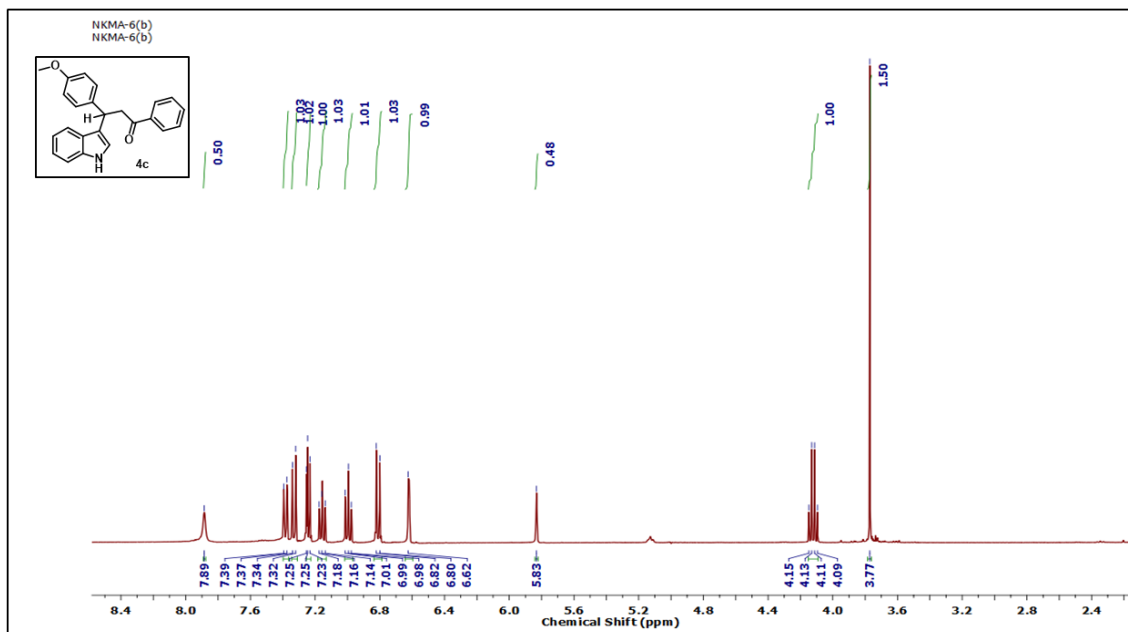


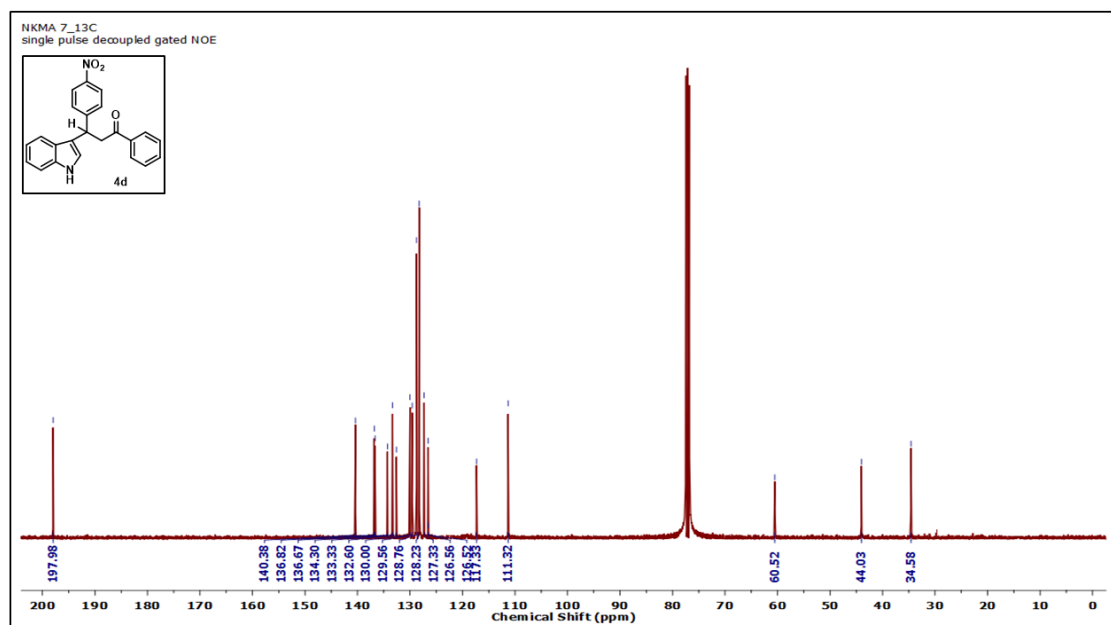
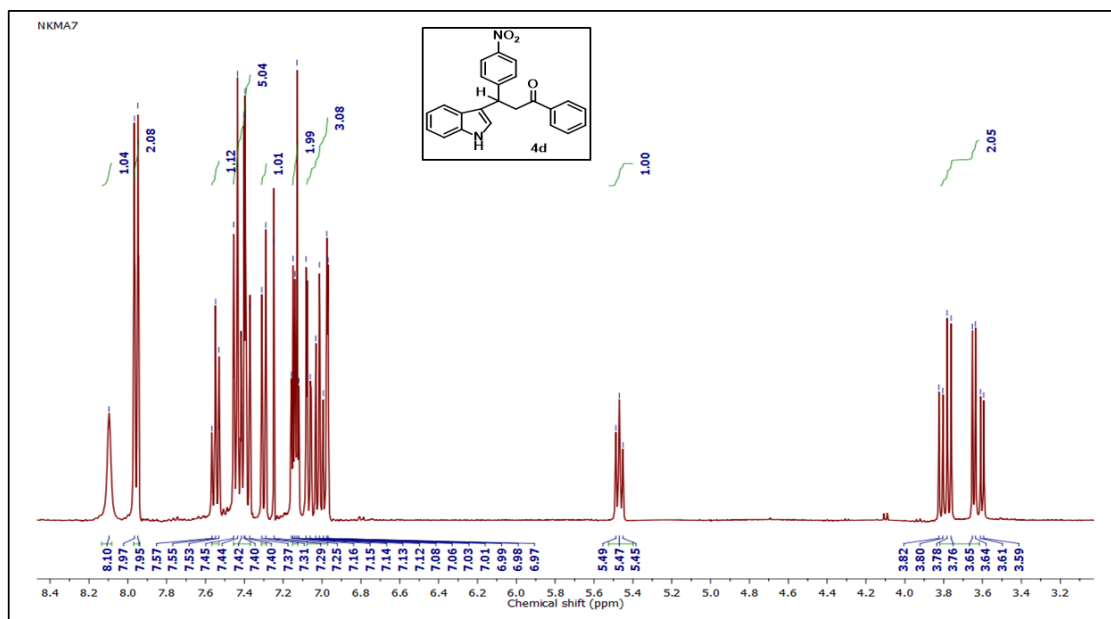


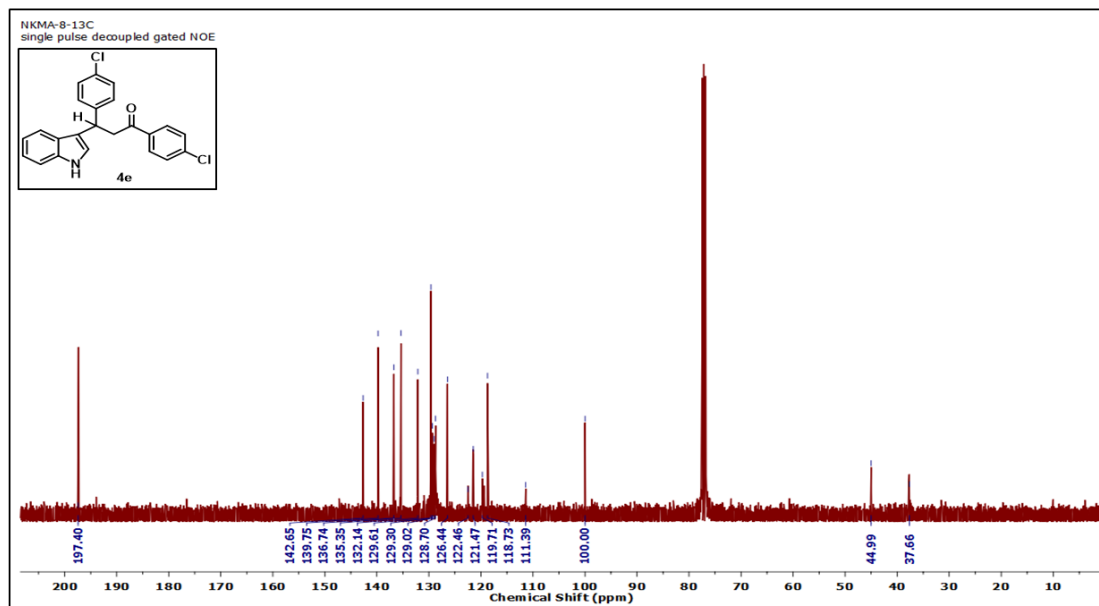
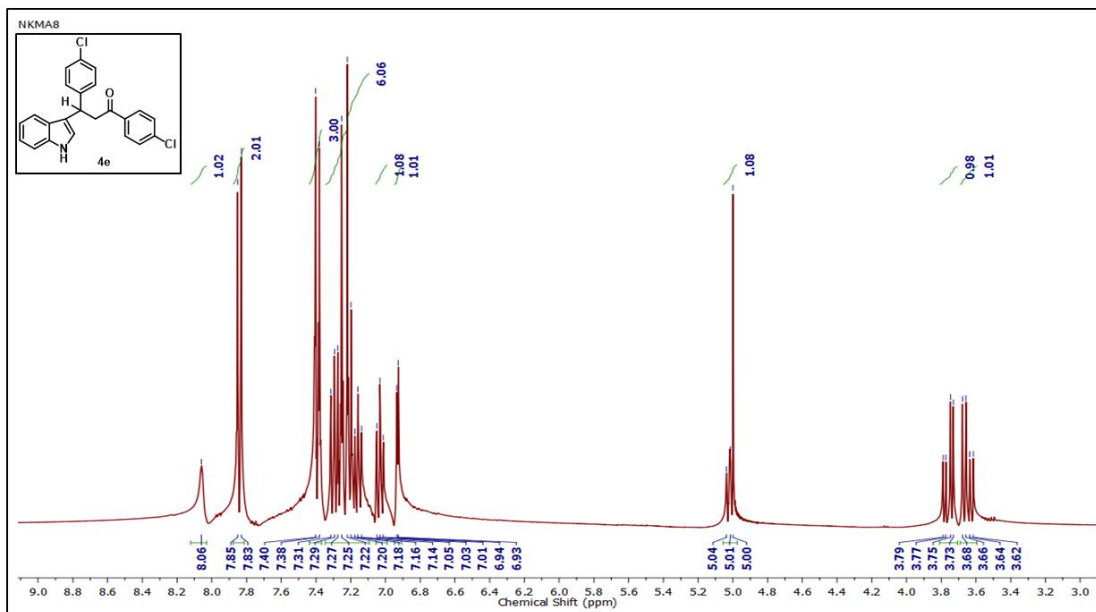


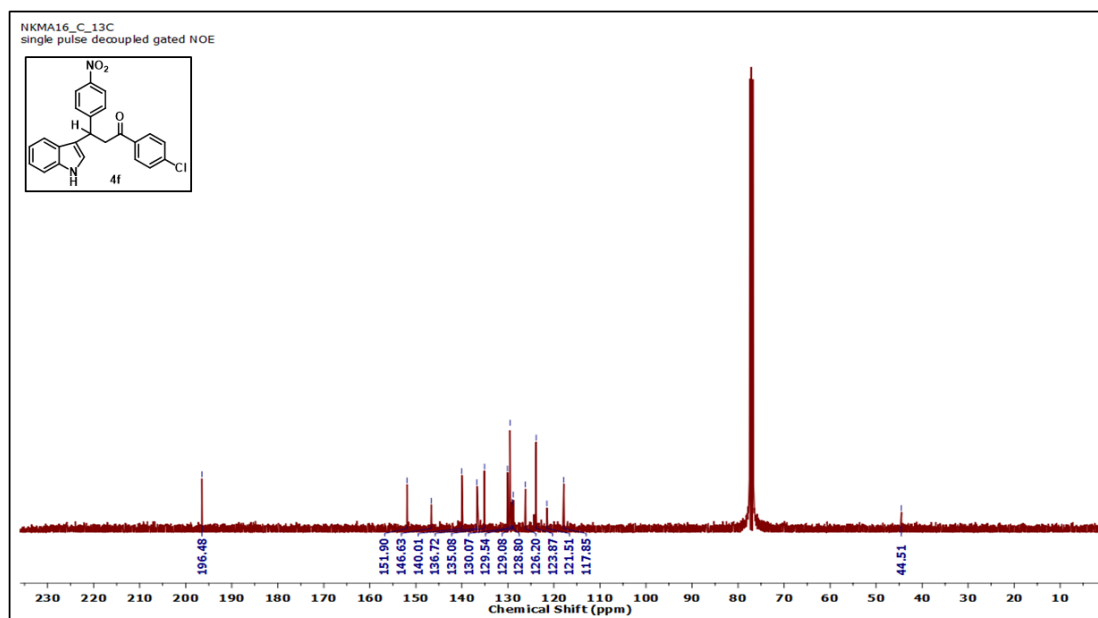
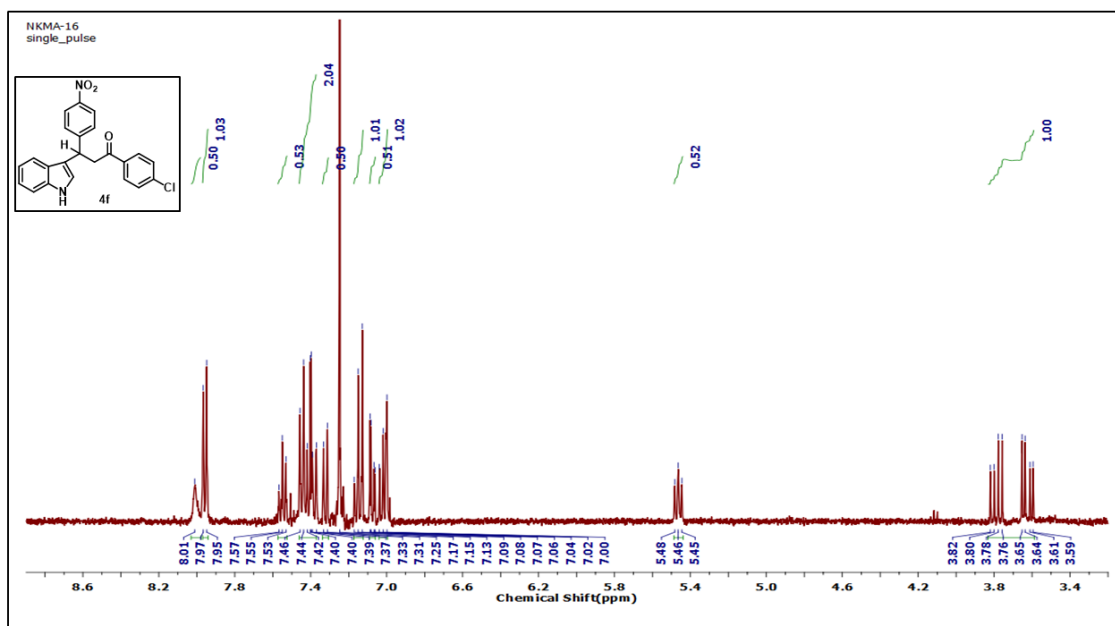


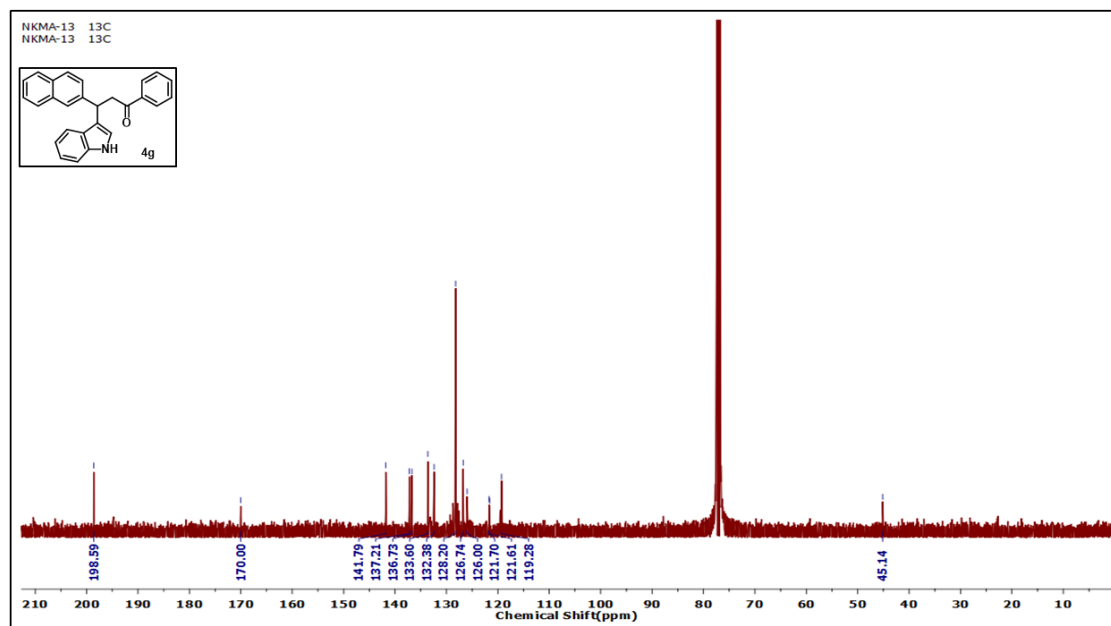
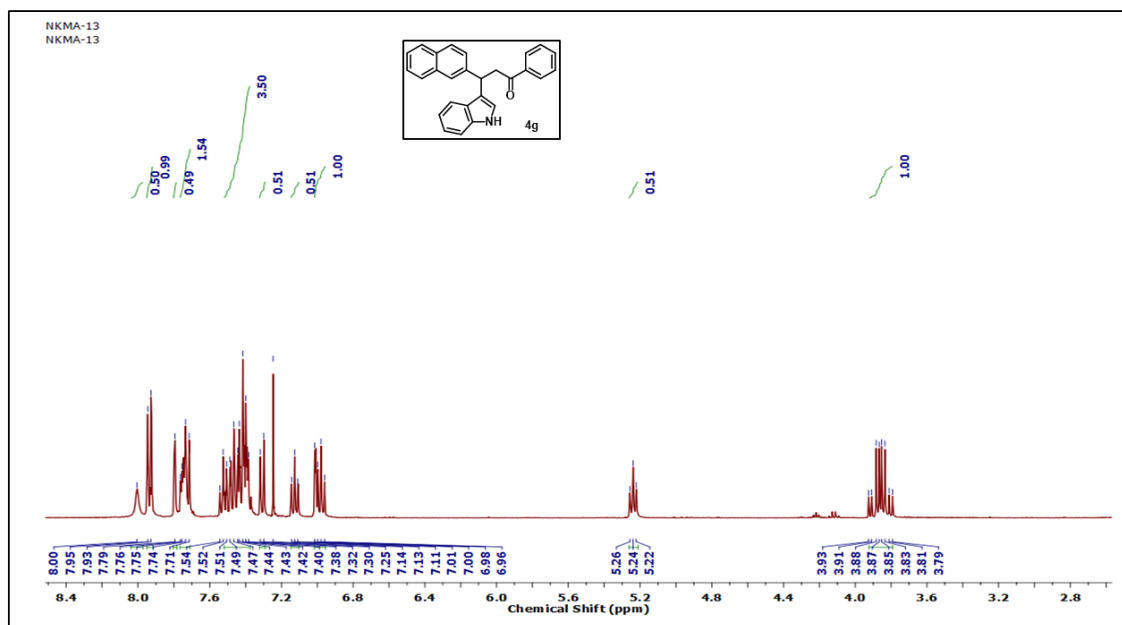












4.10 Bibliography

1. Yadav, R. N., Garcia, L., and Banik, B. K. Camphor sulfonic acid-catalyzed Michael reaction of indoles with enones. *Current Organocatalysis*, 5(3): 201-204, 2018.
2. Zhuang, C., Zhang, W., Sheng, C., Zhang, W., Xing, C. and Miao, Z. Chalcone: A privileged structure in medicinal chemistry. *Chemical Reviews*, 117(12): 7762-7810, 2017.
3. Sravanthi, T. V. and Manju, S. L. Indoles—A promising scaffold for drug

- development. *European Journal of Pharmaceutical Sciences*, 91: 1-10, 2016.
4. Lefemine, D. V., Dann, M., Barbatschi, F., Hausmann, W. K., Zbinovsky, V., Monnikendam, P., Adam, J., and Bohonos, N. Isolation and characterization mitromycin and other antibiotics. *Journal of the American Chemical Society*, 84(16): 3184-3185, 1962.
 5. Hwang, D. J., Wang, J., Li, W., and Miller, D. D. Structural optimization of indole derivatives acting at colchicine binding site as potential anticancer agents. *ACS Medicinal Chemistry Letters*, 6(9): 993-997, 2015.
 6. Von Wittenau, M. S. and Els, H. The structure of indolmycin. *Journal of the American Chemical Society*, 83(22): 4678-4680, 1961.
 7. Kerzarea, D. and Khedekar, P. Indole derivatives acting on central nervous system—review. *Journal of Pharmaceutical Science and Bioscientific Research*, 6(1): 144-156, 2016.
 8. Andersson, K. E. and Wagner, G. Physiology of penile erection. *Physiological Reviews*, 75(1): 191-236, 1995.
 9. Rosengren, A. H., Jokubka, R., Tojjar, D., Granhall, C., Hansson, O., Li, D. Q., Nagaraj, V., Reinbothe, T. M., Tuncel, J., Eliasson, L., and Groop, L. Overexpression of alpha2A-adrenergic receptors contributes to type 2 diabetes. *Science*, 327(5962): 217-220, 2010.
 10. Hollister, L. E., Overall, J. E., Katz, G., Higginbotham, W. E., and Kimbell Jr, I. Oxypertine and thiothixene in newly admitted schizophrenic patients; A further search for specific indications of antipsychotic drugs. *Clinical Pharmacology & Therapeutics*, 12(3): 531-538, 1971.
 11. Leneva, I. A., Russell, R. J., Boriskin, Y. S., and Hay, A. J. Characteristics of arbidol-resistant mutants of influenza virus: implications for the mechanism of anti-influenza action of arbidol. *Antiviral Research*, 81(2): 132-140, 2009.
 12. Modzelewska, A., Pettit, C., Achanta, G., Davidson, N. E., Huang, P., and Khan, S. R. Anticancer activities of novel chalcone and bis-chalcone derivatives. *Bioorganic & Medicinal Chemistry*, 14(10): 3491-3495, 2006.
 13. Domínguez, J. N., León, C., Rodrigues, J., Gamboa de Domínguez, N., Gut, J., and Rosenthal, P. J. Synthesis and evaluation of new antimalarial phenylurenyl chalcone derivatives. *Journal of Medicinal Chemistry*, 48(10): 3654-3658, 2005.
 14. Nielsen, S. F., Christensen, S. B., Cruciani, G., Kharazmi, A., and Liljefors, T. Antileishmanial chalcones: Statistical design, synthesis, and three-dimensional

- quantitative structure– activity relationship analysis. *Journal of Medicinal Chemistry*, 41(24): 4819-4832, 1998.
15. Yang, H. M., Shin, H. R., Cho, S. H., Bang, S. C., Song, G. Y., Ju, J. H., Kim, M. K., Lee, S. H., Ryu, J. C., Kim, Y., and Jung, S. H. Structural requirement of chalcones for the inhibitory activity of interleukin-5. *Bioorganic & Medicinal Chemistry*, 15(1): 104-111, 2007.
16. Cheenpracha, S., Karalai, C., Ponglimanont, C., Subhadhirasakul, S., and Tewtrakul, S. Anti-HIV-1 protease activity of compounds from *Boesenbergia pandurata*. *Bioorganic & Medicinal Chemistry*, 14(6): 1710-1714, 2006.
17. Svetaz, L., Tapia, A., López, S. N., Furlán, R. L., Petenatti, E., Pioli, R., Schmeda-Hirschmann, G., and Zacchino, S. A., Antifungal chalcones and new caffeic acid esters from *Zuccagnia punctata* acting against soybean infecting fungi. *Journal of Agricultural and Food Chemistry*, 52(11): 3297-3300, 2004.
18. Wang, G., Qiu, J., Xiao, X., Cao, A., and Zhou, F. Synthesis, biological evaluation and molecular docking studies of a new series of chalcones containing naphthalene moiety as anticancer agents. *Bioorganic Chemistry*, 76: 249-257, 2018.
19. Shanmugavelan, P., Sathishkumar, M., Nagarajan, S., and Ponnuswamy, A. A facile synthesis of 1, 2, 3-triazolyl indole hybrids via SbCl_3 -catalysed Michael addition of indoles to 1, 2, 3-triazolyl chalcones. *Journal of Chemical Sciences*, 124: 941-950, 2012.
20. Huang, Z. H., Zou, J. P., and Jiang, W. Q. Gallium (III) triiodide catalyzed conjugate addition of indoles with α , β -unsaturated ketones. *Tetrahedron Letters*, 47(45): 7965-7968, 2006.
21. Ekbote, S. S., Panda, A. G., Bhor, M. D., and Bhanage, B. M. Polyvinylsulfonic acid as a novel Brønsted acid catalyst for Michael addition of indoles to α , β -unsaturated ketones. *Catalysis Communications*, 10(12): 1569-1573, 2009.
22. Ji, S. J. and Wang, S. Y. Ultrasound-accelerated Michael addition of indole to α , β -unsaturated ketones catalyzed by ceric ammonium nitrate (CAN). *Synlett*, 2003(13): 2074-2076, 2003.
23. Ji, S. J. and Wang, S. Y. An expeditious synthesis of β -indolylketones catalyzed by p-toluenesulfonic acid (PTSA) using ultrasonic irradiation. *Ultrasonics Sonochemistry*, 12(5): 339-343, 2005.
24. Yadav, J. S., Abraham, S., Reddy, B. S., and Sabitha, G. InCl_3 -catalysed conjugate addition of indoles with electron-deficient olefins. *Synthesis*, 2001(14): 2165-2169,
-

- 2001.
25. Bartoli, G., Bartolacci, M., Bosco, M., Foglia, G., Giuliani, A., Marcantoni, E., Sambri, L. and Torregiani, E. The Michael addition of indoles to α , β -unsaturated ketones catalyzed by $\text{CeCl}_3 \cdot 7\text{H}_2\text{O}$ -NaI combination supported on silica gel. *The Journal of Organic Chemistry*, 68(11): 4594-4597, 2003.
26. Yu, C. J. and Liu, C. J. Conjugate Addition of Indoles to α , β -Unsaturated Ketones Using a Brønsted Acid Ionic Liquid as an Efficient Catalyst. *Molecules*, 14(9): 3222-3228, 2009.
27. Das, S., Porashar, B., Saikia, S., and Borah, R. Brønsted acidic ionic liquids catalysed sequential Michael-like addition of indole with chalcones via Claisen-Schmidt condensation. *ChemistrySelect*, 5(10): 3041-3047, 2020.
28. Heravi, M. M. and Sadjadi, S. Recent developments in use of heteropolyacids, their salts and polyoxometalates in organic synthesis. *Journal of the Iranian Chemical Society*, 6: 1-54, 2009.
29. Kozhevnikov, I. V. Catalysis by heteropoly acids and multicomponent polyoxometalates in liquid-phase reactions. *Chemical Reviews*, 98(1): 171-198, 1998.
30. Alipour, M., Akintola, O., Buchholz, A., Mirzaei, M., Eshtiagh-Hosseini, H., Görls, H., and Plass, W. Size-dependent self-assembly of lanthanide-based coordination frameworks with phenanthroline-2, 9-dicarboxylic acid as a preorganized ligand in hybrid materials. *European Journal of Inorganic Chemistry*, 2016(34): 5356-5365, 2016.
31. Heravi, M. M., Mirzaei, M., Beheshtiha, S. Y. S., Zadsirjan, V., Mashayekh Ameli, F., and Bazargan, M. $\text{H}_5\text{BW}_{12}\text{O}_{40}$ as a green and efficient homogeneous but recyclable catalyst in the synthesis of 4H-Pyrans via multicomponent reaction. *Applied Organometallic Chemistry*, 32(9): e4479, 2018.
32. Arefian, M., Mirzaei, M. and Eshtiagh-Hosseini, H. Structural insights into two inorganic-organic hybrids based on chiral amino acids and polyoxomolybdates. *Journal of Molecular Structure*, 1156: 550-558, 2018.
33. Cao, G. J., Liu, J. D., Zhuang, T. T., Cai, X. H., and Zheng, S. T. A polyoxometalate-organic supramolecular nanotube with high chemical stability and proton-conducting properties. *Chemical Communications*, 51(11): 2048-2051, 2015.

34. Lesbani, A., Kawamoto, R., Uchida, S., and Mizuno, N. Control of structures and sorption properties of ionic crystals of $A_2[Cr_3O(OOCC_2H_5)_6(H_2O)_3]_2[\alpha-SiW_{12}O_{40}]$ (A= Na, K, Rb, NH_4 , Cs, TMA). *Inorganic Chemistry*, 47(8): 3349-3357, 2008.
35. Hosseinzadeh-Baghan, S., Mirzaei, M., Eshtiagh-Hosseini, H., Zadsirjan, V., Heravi, M. M., and Mague, J. T. An inorganic–organic hybrid material based on a Keggin-type polyoxometalate@Dysprosium as an effective and green catalyst in the synthesis of 2-amino-4H-chromenes via multicomponent reactions. *Applied Organometallic Chemistry*, 34(9): e5793, 2020.
36. Neumann, R. and Levin, M. Aerobic oxidative dehydrogenations catalyzed by the mixed-addenda heteropolyanion $PV_2Mo_{10}O_{40}^{5-}$: A kinetic and mechanistic study. *Journal of the American Chemical Society*, 114(18): 7278-7286, 1992.
37. Lissel, M., in de Wal, H. J., and Neumann, R. Oxidation of activated phenols by dioxygen catalysed by the $H_5PV_2Mo_{10}O_{40}$ heteropolyanion. *Tetrahedron Letters*, 33(13): 1795-1798, 1992.
38. Linguito, S. L., Zhang, X., Padmanabhan, M., Biradar, A.V., Xu, T., Emge, T. J., Asefa, T., and Li, J. New polyoxomolybdate compounds synthesized in situ using ionic liquid 1-butyl-3-methyl-imidazolium tetrafluoroborate as green solvent. *New Journal of Chemistry*, 37(9): 2894-2901, 2013.
39. Wang, H., Chen, Y. P., You, Z. C., Zhou, M. X., Zhang, N., and Sun, Y. Q. Synthesis and characterization of a new catalyst for RhB degradation constructed by $[SiMo_{12}O_{40}]^{4-}$ anionic cluster. *Chinese Chemical Letters*, 26(2): 187-192, 2015.
40. Macht, J., Janik, M. J., Neurock, M., and Iglesia, E. Catalytic consequences of composition in polyoxometalate clusters with Keggin structure. *Angewandte Chemie International Edition*, 46(41): 7864-7868, 2007.
41. Heravi, M. M., Hosseinejad, T., Tamimi, M., Zadsirjan, V., and Mirzaei, M. 12-Tungstoboric acid ($H_5BW_{12}O_{40}$) as an efficient Lewis acid catalyst for the synthesis of chromenopyrimidine-2, 5-diones and thioxochromenopyrimidin-5-ones: Joint experimental and computational study. *Journal of Molecular Structure*, 1205: 127598, 2020.
42. Ren, Y., Wang, M., Chen, X., Yue, B., and He, H. Heterogeneous catalysis of polyoxometalate based organic–inorganic hybrids. *Materials*, 8(4): 1545-1567, 2015.

43. Derakhshanrad, S., Mirzaei, M., Streb, C., Amiri, A., and Ritchie, C. Polyoxometalate-based frameworks as adsorbents for drug of abuse extraction from hair samples. *Inorganic Chemistry*, 60(3): 1472-1479, 2021.
44. Akbari, M., Mirzaei, M., and Amiri, A. Synergistic effect of lacunary polyoxotungstates and carbon nanotubes for extraction of organophosphorus pesticides. *Microchemical Journal*, 170: 106665, 2021.
45. Amiri, A., Mirzaei, M., and Derakhshanrad, S. A nanohybrid composed of polyoxotungstate and graphene oxide for dispersive micro solid-phase extraction of non-steroidal anti-inflammatory drugs prior to their quantitation by HPLC. *Microchimica Acta*, 186: 1-7, 2019.
46. Misra, A., Kozma, K., Streb, C., and Nyman, M. Beyond charge balance: counter-cations in polyoxometalate chemistry. *Angewandte Chemie International Edition*, 59(2): 596-612, 2020.
47. Poli, E., De Sousa, R., Jerome, F., Pouilloux, Y., and Clacens, J. M. Catalytic epoxidation of styrene and methyl oleate over peroxophosphotungstate entrapped in mesoporous SBA-15. *Catalysis Science & Technology*, 2(5): 910-914, 2012.
48. Yamaguchi, K., Yoshida, C., Uchida, S., and Mizuno, N. Peroxotungstate immobilized on ionic liquid-modified silica as a heterogeneous epoxidation catalyst with hydrogen peroxide. *Journal of the American Chemical Society*, 127(2): 530-531, 2005.
49. Malmir, M., Heravi, M. M., Yekke-Ghasemi, Z., and Mirzaei, M. Incorporating heterogeneous lacunary Keggin anions as efficient catalysts for solvent-free cyanosilylation of aldehydes and ketones. *Scientific Reports*, 12(1): 11573, 2022.
50. Yekke-Ghasemi, Z., Heravi, M. M., Malmir, M., Jahani, G., Bisafar, M. B., and Mirzaei, M. Fabrication of heterogeneous-based lacunary polyoxometalates as efficient catalysts for the multicomponent and clean synthesis of pyrazolopyranopyrimidines. *Inorganic Chemistry Communications*, 140: 109456, 2022.
51. Daraie, M., Heravi, M. M., Mirzaei, M., and Lotfian, N. Synthesis of pyrazolo-[4, 3: 5, 6] pyrido [2, 3-d] pyrimidine-diones catalyzed by a nano-sized surface-Grafted neodymium complex of the tungstosilicate via multicomponent reaction. *Applied Organometallic Chemistry*, 33(9): e5058, 2019.
52. Heravi, M. M., Momeni, T., Mirzaei, M., Zadsirjan, V., and Tahmasebi, M. An amino acid@ isopolyoxometalate nanoparticles catalyst containing aspartic acid

- and octamolybdate for the synthesis of functionalized spirochromenes. *Inorganic and Nano-Metal Chemistry*, 51(6): 896-909, 2021.
53. Ghanbarian, M., Beheshtiha, S. Y. S., Heravi, M. M., Mirzaei, M., Zadsirjan, V., and Lotfian, N. A nano-sized Nd–Ag@ polyoxometalate catalyst for catalyzing the multicomponent Hantzsch and Biginelli reactions. *Journal of Cluster Science*, 31: 1295-1306, 2020.
54. Daraie, M., Mirzaei, M., Bazargan, M., Amiri, V. S., Sanati, B. A., and Heravi, M. M. Lanthanoid-containing polyoxometalate nanocatalysts in the synthesis of bioactive isatin-based compounds. *Scientific Reports*, 12(1): 12004, 2022.
55. Lotfian, N., Heravi, M. M., Mirzaei, M., and Daraie, M. Investigation of the uncommon basic properties of $[\text{Ln}(\text{W}_5\text{O}_{18})_2]^{9-}$ (Ln= La, Ce, Nd, Gd, Tb) by changing central lanthanoids in the syntheses of pyrazolopyranopyrimidines. *Journal of Molecular Structure*, 1199: 126953, 2020.
56. Skoda-Földes, R. The use of supported acidic ionic liquids in organic synthesis. *Molecules*, 19(7): 8840-8884, 2014.
57. Masri, A. N., Mi, A. M., and Leveque, J. M. Industrial Engineering & Management. Volume 5, page 197, 2016.
58. Bridgeman, A. J. Density functional study of the vibrational frequencies of α -Keggin heteropolyanions. *Chemical Physics*, 287(1-2): 55-69, 2003.
59. Seki, T., Chiang, K. Y., Yu, C. C., Yu, X., Okuno, M., Hunger, J., Nagata, Y., and Bonn, M. The bending mode of water: A powerful probe for hydrogen bond structure of aqueous systems. *The Journal of Physical Chemistry Letters*, 11(19): 8459-8469, 2020.
60. Rajkumar, T. and Ranga Rao, G. Investigation of hybrid molecular material prepared by ionic liquid and polyoxometalate anion. *Journal of Chemical Sciences*, 120: 587-594, 2008.
61. Rao, G. R. and Rajkumar, T. Interaction of Keggin anions of 12-tungstophosphoric acid with $\text{Ce}_x\text{Zr}_{1-x}\text{O}_2$ solid solutions. *Journal of Colloid and Interface Science*, 324(1-2): 134-141, 2008.
62. de Oliveira Jr, M., Rodrigues-Filho, U. P., and Schneider, J. Thermal transformations and proton species in 12-phosphotungstic acid hexahydrate studied by ^1H and ^{31}P solid-state nuclear magnetic resonance. *The Journal of Physical Chemistry C*, 118(22): 11573-11583, 2014.
63. Bridgeman, A. J. Computational Study of the Vibrational Spectra of α - and β -

-
- Keggin Polyoxometalates. *Chemistry–A European Journal*, 10(12): 2935-2941, 2004.
64. Rao, G. R., Rajkumar, T., and Varghese, B. Synthesis and characterization of 1-butyl 3-methyl imidazolium phosphomolybdate molecular salt. *Solid State Sciences*, 11(1): 36-42, 2009.
65. Ji, Y., Shi, R., Wang, Y., and Saielli, G. Effect of the chain length on the structure of ionic liquids: From spatial heterogeneity to ionic liquid crystals. *The Journal of Physical Chemistry B*, 117(4): 1104-1109, 2013.
66. Noda, L. K., de Almeida, R. M., Probst, L. F. D., and Gonçalves, N. S. Characterization of sulfated TiO₂ prepared by the sol–gel method and its catalytic activity in the n-hexane isomerization reaction. *Journal of Molecular Catalysis A: Chemical*, 225(1): 39-46, 2005.
67. Huque, F. T. and Platts, J. A. The effect of intramolecular interactions on hydrogen bond acidity. *Organic & Biomolecular Chemistry*, 1(8): 1419-1424, 2003.
68. Qian, C., Li, X., and Zhang, M. Arene diazonium tetrafluoroborate salts: Novel Lewis acid catalysts for Friedel-Crafts alkylation of indoles with α , β -unsaturated ketones. *ChemistrySelect*, 8(9): e202204860, 2023.
69. Dave, A. Y., Mishra, A., Talukdar, M., and Begari, E. Eucalyptol: An alternative green solvent for the Michael addition of indoles to α , β -unsaturated ketones and nitrostyrenes. *ChemistrySelect*, 7(25): e202200954, 2022.
70. Zhang, X., Jones-Mensah, E., Deobald, J., and Magolan, J. Alkylation of indoles with α , β -unsaturated ketones using alumina in hexanes. *Advanced Synthesis & Catalysis*, 361(24): 5548-5551, 2019.
71. Zeng, X. F., Ji, S. J., and Shen, S. S. Conjugate addition of indoles to α , β -unsaturated ketones (Chalcones) catalyzed by KHSO₄ under ultrasonic conditions. *Chinese Journal of Chemistry*, 25(12): 1777-1780, 2007.
72. Gumerova, N. I. and Rompel, A.. Polyoxometalates in solution: speciation under spotlight. *Chemical Society Reviews*, 49(21): 7568-7601, 2020.
73. van Veen, J. R., Sudmeijer, O., Emeis, C. A., and de Wit, H. On the identification of molybdophosphate complexes in aqueous solution. *Journal of the Chemical Society, Dalton Transactions*, (9): 1825-1831, 1986.
-